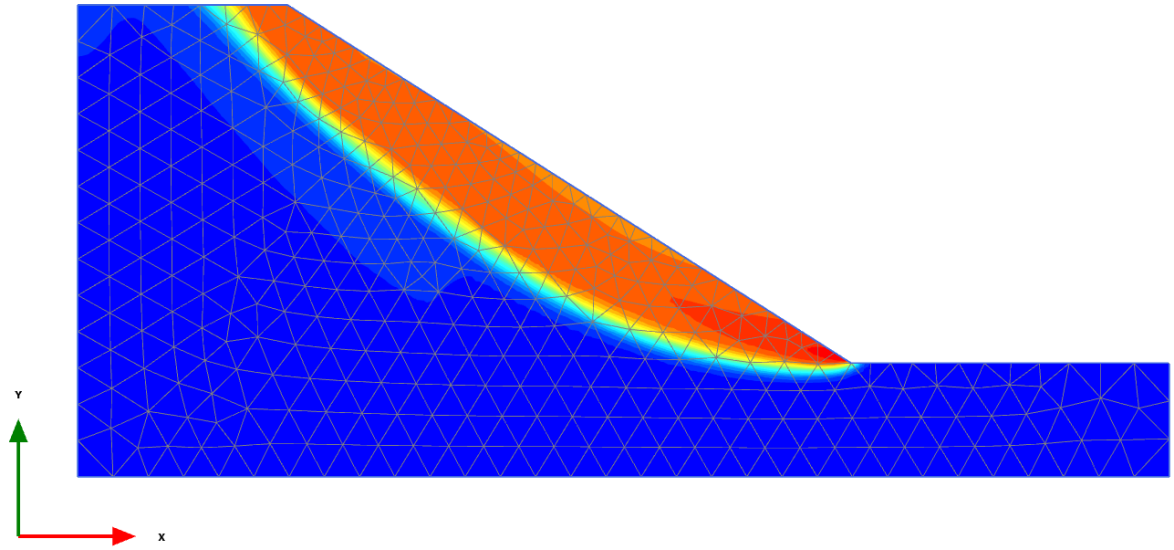

Effect of the soil water characteristic curve on the stability of partially saturated slopes

Safety analysis of unsaturated slopes under infiltration using PLAXIS 2D-Remote Scripting

Master's thesis in Master Program Infrastructure and Environmental Engineering

Akshaya Shankar

Department of Architecture and Civil Engineering
Division of Geology and Geotechnics
CHALMERS UNIVERSITY OF TECHNOLOGY
Master's Thesis ACEX30
Gothenburg,Sweden 2024
www.chalmers.se

Master's thesis ACEX30

Effect of the soil water characteristic curve on the stability of partially saturated slopes

Safety analysis of unsaturated slopes under infiltration using PLAXIS 2D- Remote Scripting

AKSHAYA SHANKAR

CHALMERS
UNIVERSITY OF TECHNOLOGY

Department of Architecture and Civil Engineering
Division of Geology and Geotechnics
Chalmers University of Technology
Gothenburg, Sweden 2024

Effect of the soil water characteristic curve on the stability of partially saturated slopes
Safety analysis of unsaturated slopes under infiltration using PLAXIS 2D- Remote Scripting
Akshaya Shankar

Examensarbete ACEX30
Institutionen för arkitektur och samhällsbyggnadsteknik
Chalmers tekniska högskola, 2024

Department of Architecture and Civil Engineering
Division of Geology and Geotechnics
Chalmers University of Technology
SE-412 96 Gothenburg
Telephone +46 31 772 1000

Cover: An illustration of total displacement of slope section under gravity loading

Department of Architecture and Civil Engineering
Gothenburg, Sweden 2024

Effect of the soil water characteristic curve on the stability of partially saturated slopes
Safety analysis of unsaturated slopes under infiltration using PLAXIS 2D- Remote Scripting
AKSHAYA SHANKAR
Department of Architecture and Civil Engineering
Chalmers University of Technology

Abstract

Rainfall significantly contributes to slope failure in unsaturated slopes by causing a reduction in matrix suction and subsequent decline in shear strength of the soil. Understanding the relationship between matrix suction and moisture content is crucial for describing the hydraulic behavior of unsaturated soil, typically represented by the Soil-Water Characteristic Curve (SWCC). This study focuses on assessing how SWCC affects the stability of partially saturated soil during infiltration using fully coupled-flow deformation analysis in PLAXIS 2D. To enhance efficiency and automate analyses for numerous iterations, PLAXIS-remote scripting is utilized.Parameters that quantify the SWCC are utilized to depict the properties of unsaturated soils. The Van- Genuchten parameters, which describe the hydraulic behavior of unsaturated soil, have been determined based on the SWCC. Furthermore, the impact of Van Genuchten parameters (g_a , g_n) that best fit the SWCC on the stability of unsaturated soil under rainfall conditions has been studied. The slope stability under infiltration is initially examined based on the derived VG parameters. Subsequently, the impact of VG parameters on the stability of unsaturated slopes is assessed by determining five different values for each parameter:g_a and g_n. These values are utilized to generate five unique sets of VG parameters, resulting in 25 combinations. The stability of the unsaturated slope under the effect of rainfall is then evaluated for these 25 combinations of VG parameters. In addition to hydraulic parameters, factors such as the geometry of the slope and the shear strength properties of the soil also play a significant role in influencing the stability of unsaturated slopes. Therefore, a sensitivity analysis is conducted by varying the slope geometry and shear strength properties to explore the impact of 25 different combinations of Van Genuchten parameters. The resulting values of FOS are then compared with the original slope geometry and shear strength properties for all 25 combinations of Van Genuchten parameters under the effect of rainfall, in order to investigate the slope stability.Upon increasing the values of g_a and g_n, the FOS of the slope significantly decreases under the influence of rainfall. Moreover, sensitivity analysis results indicate that the stability of an unsaturated slope under consistent rainfall infiltration is directly correlated with the VG parameters and shear strength parameters, while being inversely proportional to the slope's geometry.

Keywords: Unsaturated Slope, SWCC, matrix suction, fully coupled flow-deformation analysis, FOS, PLAXIS 2D, remote scripting, python codes.

Acknowledgements

The study examines how the SWCC influences the stability of unsaturated silt slopes when subjected to rainfall. This master's thesis forms a part of the Infrastructure and Environmental Programme at Chalmers University of Technology in Gothenburg. The research was conducted within the Geology and Geotechnics division under the guidance of Ayman Abed, a senior lecturer in the Department of Geotechnics at Chalmers University. The study was conducted in the spring semester, spanning from January to June 2024.

I am incredibly grateful for the exceptional support and guidance provided by my supervisor, Ayman Abed, who also conceived the thesis topic. Your constant presence and assistance in overcoming the challenges during this investigation are greatly appreciated. Additionally, I would like to extend my heartfelt gratitude to my examiner, Minna Karstunen, the Head of Division and Professor of Geology and Geotechnics at Chalmers University of Technology. Your valuable feedback and insights for the project have been invaluable and are sincerely appreciated.

I would like to extend my gratitude to my opponents, Zaki Alzaki and Muhammad Asad, for the engaging discussions on the subject, the productive Zoom meeting, and their valuable feedback on my work.

Finally, I would like to thank my family for their immense support throughout my journey of conducting this thesis investigation

Akshaya Shankar, Gothenburg, June 2024

Contents

List of Figures

List of Tables

List of Notations

Abbreviations

SWCC	Soil water characteristic curves
AEV	Air-entry value
VG	Van-Genuchten
FOS	Factor of safety
API	Application Programming Interface
DMT	Dilatometer Test
CPT	Cone Penetration Test
USDA	United States Department of Agriculture

Greek Symbols

ρ_w	density of water
α_1	contact angle
π	osmotic suction
ψ	total suction
θ	volumetric water content
$w(\psi)$	water content to corresponding soil suction
$C(\psi)$	correction factor
θ_n	normalised volumetric water content
θ_r	residual volumetric water content
θ_s	saturated volumetric water content
$K_r(\psi)$	relative coefficient of permeability
K_s	saturated coefficient of permeability
$K_w(\psi)$	coefficient of permeability at soil suction
σ, σ_v	Total stress
σ', σ'_v	Effective stress
$\sigma - u_a$	net normal stress
χ	Soil parameter
τ_{xy}	shear stress on the x-face in the y-direction

τ_{xz}	shear stress on the x-face in the z-direction
τ_{yz}	shear stress on the y-face in the z-direction
τ_{yx}	shear stress on the y-face in the x-direction
τ_{zx}	shear stress on the z-face in the x-direction
τ_{zy}	shear stress on the z-face in the y-direction
γ_w	unit weight of water
γ_{unsat}	unsaturated unit weight of soil
γ_{sat}	saturated unit weight of soil
τ	equilibrium shear stress
ϕ_d	friction angle in total stress
ϕ'	friction angle in effective stress
ρ_{bulk}	Bulk density of soil
υ	Poisson's ratio
Φ_p	Pressure Head

Roman Symbols

h_c	capillary pressure head
T_s	surface tension
R_s	radius of curvature of the meniscus
r	radius of the capillary tube
p_c	capillary pressure
p_{air}	air pressure
p_{water}	water pressure
g	gravitational constant
u_a -u_w	matric suction
w	gravimetric water content
M_w	mass of water
M_s	mass of solids
V_v	volume of voids
V_s	volume of solids
V_w	volume of water
w_s	saturated water content
a,n,m	curve fitting parameters
a_{m1},a_{m2}	curve fitting parameters
n_{m1},n_{m2}	curve fitting parameters
S_e	effective saturation
u_w	Pore water pressure
F	Factor of safety
s	available shear strength
c_d	cohesion in total stress
c'	cohesion in effective stress

,

k_x	Saturated permeability in horizontal direction
k_y	Saturated permeability in vertical direction
d_{10}	effective size of the soil particle
g_a, g_n, g_m	Van-Genuchten curve fitting parameters used in PLAXIS 2D
g_l	Empirical parameter
S_{sat}	degree of saturation at fully saturated conditions
S_{res}	degree of saturation at residual conditions
n	Porosity of the soil
e	void ratio
G	Specific gravity of soil
w	moisture content
E'_{ref}	Modulus of Elasticity

1

Introduction

1.1 Background

The stability of the slopes are generally governed by the strength of the unsaturated soil (Gofar and Rahardjo, 2016). Unsaturated soil mechanics did not evolve concurrently with saturated soil mechanics; rather, it was gradually integrated into soil mechanics through a variety of theoretical and practical investigations (Delwyn.G.Fredlund et al., 2012). Unsaturated soil is identified by the existence of four distinct phases: the solid phase, water phase, air phase and air-water interface phase. Changes in the stress states of this interface, which functions as a thin layer bonded around voids, can ideally result in changes to the volume, degree of saturation and shear strength. In general there are two zones in a soil profile: unsaturated and saturated zones (Öberg, 1997). The unsaturated zone is the region between the water table and the ground surface which comprises three sub zones namely, capillary zone, vadose zone and dry zone. The capillary zone is located just above the water table where the soil pores are filled by air and water under the action of capillary forces. The dry zone is located near the ground surface. During infiltration the pores in the dry zone are completely saturated by water and gravity forces causes the water to move further down to the vadose zone. Longer-periods of infiltration raises the groundwater table resulting in increase in pore water pressure (Cai and Ugai, 2004). When the pore water pressure is lower than the atmospheric pressure it develops a negative pressure known as soil suction. Increase in pore water pressure and decrease in matrix suction caused by infiltration into unsaturated soil affects the shear strength properties thereby causing slope failures. The hydraulic conductivity and shear strength of unsaturated soil are often influenced by suction. The relationship between suction and gravimetric water content is represented by soil-water characteristic curves (SWCC). The SWCC is generally sigmoidal in shape which can be utilised to evaluate the properties of unsaturated soil (Abed and Vermeer, 2006). Suction increases with soil drying and decreases with soil wetting.

Although suction has a significant effect on the shear strength properties of unsaturated soil, negative pore water pressure was ignored in soil mechanics practices (Delwyn.G.Fredlund et al., 2012). The saturated behaviour of soil with positive pore water pressure was the primary interest of geotechnical engineers since they believed it would ensure conservative design. Bishop (1959) formulated effective stress equations for fully saturated to unsaturated soil where the net normal stress is equated to matrix suction using a soil parameter. Plaxis implements Bishop's effective stress

equation effectively, and the software additionally considers slope deformation under stress (Gofar and Rahardjo, 2016). Thus, the mechanical behaviour of unsaturated silty slopes under the effects of rainfall will be numerically investigated using Plaxis.

1.2 Aim and Objectives

The aim of this thesis is to examine the water retention behaviour of unsaturated soil under infiltration conditions, as the stability of unsaturated slopes is strongly connected to matrix suction and seasonal changes. To evaluate the influence of soil water characteristics on the stability of unsaturated soil slopes, a fully-coupled flow deformation analysis will be conducted using finite element tool such as Plaxis 2D.

The following objectives are the focus of the thesis:

- Interpretation of geotechnical properties of the slope using the given laboratory triaxial test results.
- Determination of soil permeability from grain size distribution curves.
- Derive input parameters for Mohr-coulomb constitutive model.
- Determination of hydraulic parameters by fitting them in SWCC curves using Van-Genuchten formula used in Plaxis.
- Modelling the soil profile of the slope in Plaxis and performing fully-coupled flow deformation analysis.
- Determination of factor of safety for the unsaturated slope.
- Determination of the influence of suction in unsaturated soil from pore water pressure values.
- Performing a sensitivity analysis on the slope parameters.

1.3 Limitations

Several constitutive models have been established to describe the hydro-mechanical behaviour of unsaturated soil, including the Barcelona Basic Model (BBM) and elastoplastic constitutive models, which are divided into three types based on the stress state variables such as suction and net stress, effective stress and degree of saturation, and suction and effective stress (lin Xiong et al., 2019). Nevertheless the thesis demonstrates the behaviour of unsaturated soil using the Mohr-Coulomb model. Since the choice of constitutive model can have a considerable impact on the results, using different models could vary the results.

The SWCCs are used to determine the soil suction of unsaturated soil. It is challenging to get a single suction value because SWCC is a hysteric that represents drying and wetting of unsaturated soil (Delwyn.G.Fredlund et al., 2012). Although, numerous equations have been proposed that optimise the water content verse soil suction, Plaxis has only established the Van-Genuchten model to describe the groundwater

flow in unsaturated soil. So, its a drawback to use just one model for the investigation. Furthermore, the thesis does not attempt to make a comparison between Plaxis's output with the results of other computational software programmes.

1.4 Thesis Structure

The thesis's structure initiates with an extensive literature review to comprehend the underlying principles of unsaturated soil mechanics and and its behaviour. The soil parameters for each layer of the slope profile is estimated using field measurements and laboratory data provided. The Van-Genuchten (VG) parameters will be determined by interpreting the SWCC data for each soil layer.

The interpretation of Van Genuchten (VG) parameters using SWCC involves employing an empirical equation. While the general equation for solving VG parameters focuses on delineating the relationship between volumetric water content and water potential, PLAXIS software utilizes a slightly modified approach to this equation which is tailored to meet software's functionalities and user needs. Despite the adjustments made in PLAXIS, the underlying principles guiding the equation's formulation and the relationships it encapsulates remain unchanged. In PLAXIS 2D, the VG equation utilizes a correlation between degree of saturation and pressure head to characterize the hydraulic behavior of unsaturated soil. The Van Genuchten equation from the Plaxis material model has been implemented in a Jupyter notebook for determining the VG parameters. The degree of saturation and pressure head data derived from laboratory data are utilized to construct SWCC plots. Python code is employed to generate graphs ensuring a precise fit of parameters to the SWCC, facilitating the extraction of VG parameters from the curves.

After determining the material and groundwater flow parameters for each soil layer, the slope profile will be modelled in Plaxis. Further, a fully coupled flow-deformation analysis will be carried out in Plaxis to investigate the development of pore pressures and deformations in saturated and unsaturated soils due to time-dependent variations in hydraulic boundary conditions such as infiltration. Further, the factor of safety for the unsaturated slope under the influence of rainfall will be investigated and the results are then validated.

The study also entails exploring the impact of varying each Van Genuchten parameter on the stability of silty slopes by iterating the factor of safety for different parameter sets. Additionally, it highlights the influential parameters and identifies those that cause significant changes to slope stability. Given the extensive datasets and time-consuming nature of the analysis, conducting it via PLAXIS remote scripting is the preferred approach. The analysis is fully automated using Python scripting within PLAXIS 2D. Python codes are typically interpreted within software like PLAXIS 2D through an Application Programming Interface (API). An API serves as a mechanism facilitating communication between two separate software systems by employing a predefined set of protocols. Additionally, a sensitivity analysis is being conducted on the strength parameters and geometry of the slope to examine

how they affect the factor of safety and the slope's stability during the event of rainfall. The thesis workflow is depicted through a flowchart as illustrated in *figure 1.1*

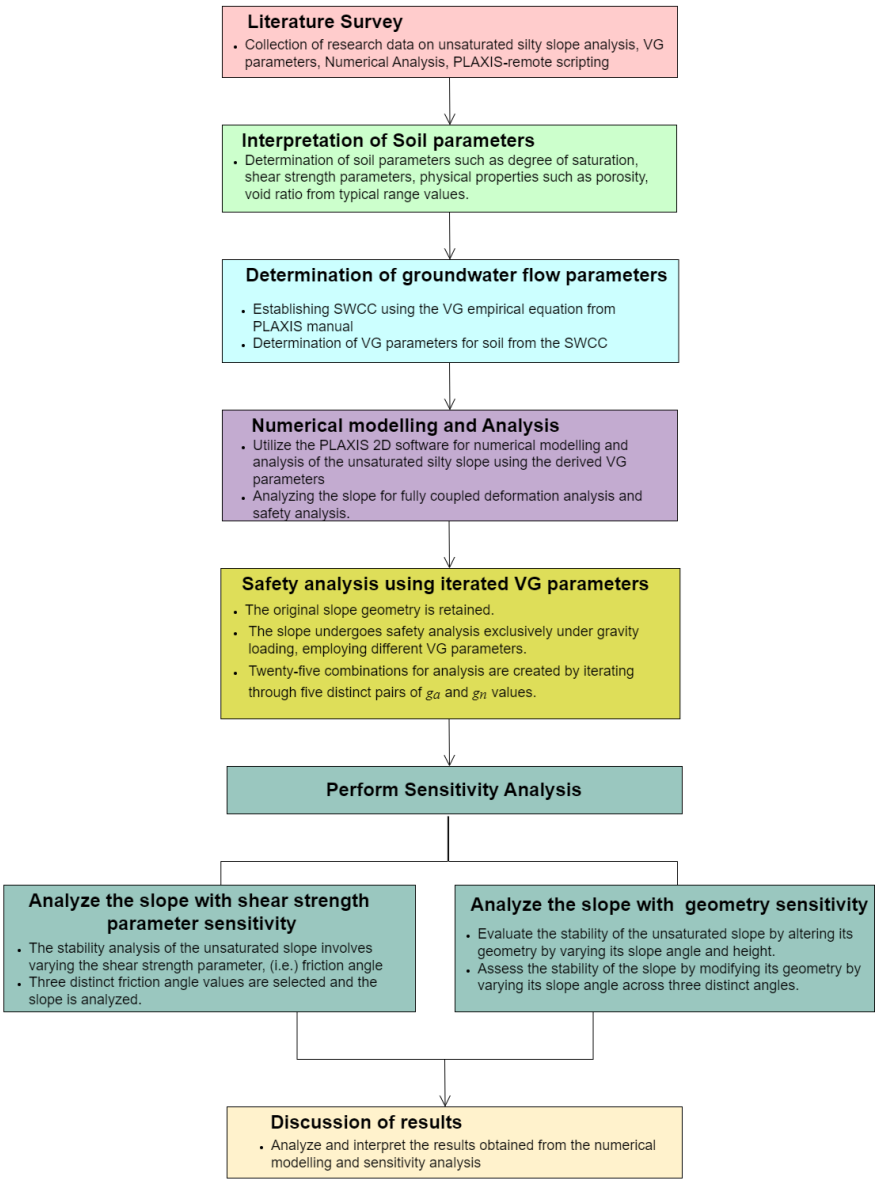

Figure 1.1: Schematic view of Methodology

2

Theory

This section illustrates the fundamental theory behind groundwater flow in unsaturated soil and the effect of suction due to capillary forces. A comprehensive literature study was performed to emphasise the properties of unsaturated soil and the significance of the soil-water characteristic curve. Additionally, the principle of effective stress developed by Terzaghi and Bishop has been addressed to identify the ideal approach for interpreting the behaviour of unsaturated soil.

2.1 Unsaturated soil mechanics

Soil mechanics combines engineering mechanics with the behaviour and properties of soil. Soil mechanics primarily focuses on the conventional types of soils, which include dry sand, silt and clays, and saturated sand, despite the fact there are several types of soil that are met in practice (Delwyn.G.Fredlund et al., 2012). Both the saturated and dry soils are two-phase systems where the dry soil consists of soil particles and pore air while saturated soil consists of soil particles and pore water. Therefore, the existence of more than one fluid phases leads to complex soil behaviour which is inconsistent with the principles used in conventional saturated soil mechanics. Unsaturated soils, in contrast to saturated soils, consist of more than two phases: the soil phase, liquid phase, gaseous phase, and air-water interface as shown in *Figure 2.1.* The air-water interface functions as a contractile skin that creates a separating barrier between the air and water, thereby making it possible to measure the degree of saturation. Due to the fundamental differences in the material structure and its behaviour it is important to understand the distinction between unsaturated and saturated soil.

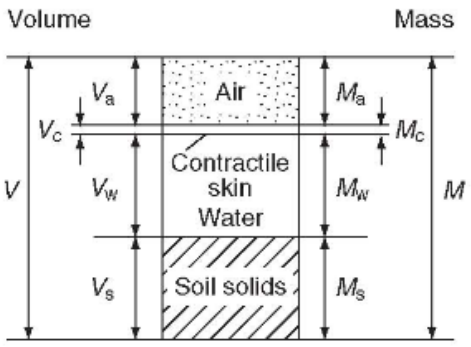

Figure 2.1: Phase diagram of unsaturated soil (Delwyn.G.Fredlund et al., 2012)

According to soil mechanics, there are saturated and unsaturated zones in every soil profile (Delwyn.G.Fredlund et al., 2012). The zone that lies between the phreatic line and the ground surface is unsaturated, whereas the zone below the phreatic line is saturated. The thickness of the unsaturated zone is determined by the position of groundwater table. As seen in the *Figure 2.2*, the unsaturated zone is further divided into three zones: the dry zone, the two-phase zone, and the capillary zone. The zone that is located directly above the groundwater table is capillary zone. The soil pores in this zone is filled with water under the influence of capillary forces. The saturation level in this zone is slightly above 90%, however it is not completely saturated due to the presence of some air bubbles in the voids. Thus, the capillary zone has continuous water phase and discontinuous air phase. The depth of the capillary zone is greatly influenced by the grain size distribution, soil type and relative density. The zone that is significantly closer to the ground surface is known as dry zone. Due to transpiration and evaporation, the zone is often drier and has a degree of saturation less than 15%. During dry periods, the available water in this zone is typically absorbed and retained together by the soil particles thus the soil pores are primarily filled with air. As a result, the air phase in this zone is continuous, whereas the water phase is discontinuous. The soil layer located between the dry and capillary zone is known as two-phase zone. The soil pores are filled with air and water. As a result, both the air and water phase are continuous in this zone. The degree of saturation in this zone typically ranges between 15% to 90%.

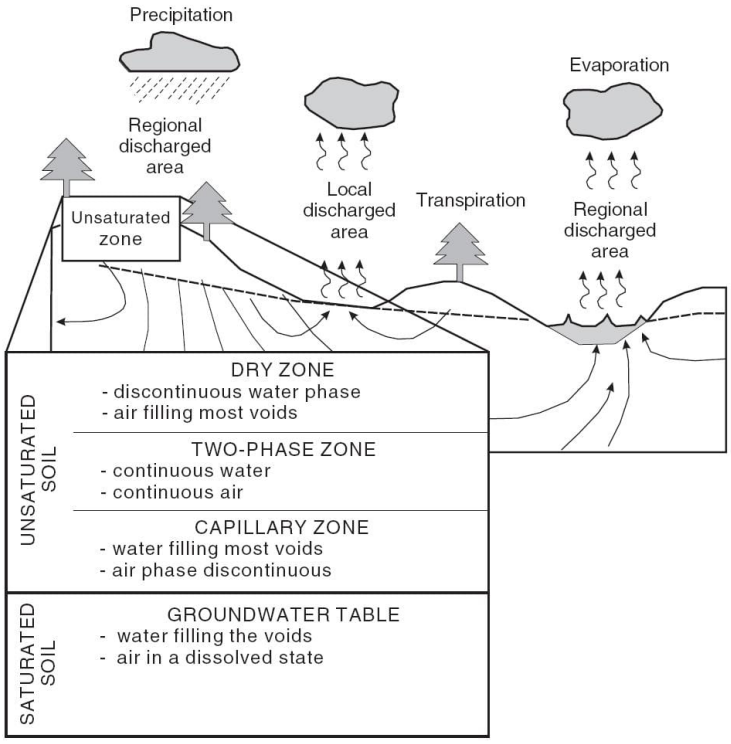

Figure 2.2: Different zones of unsaturated soil (Delwyn.G.Fredlund et al., 2012)

2.2 Groundwater flow in unsaturated soil

The behaviour of unsaturated soil is greatly influenced by the depth of groundwater table, capillary forces which causes migration of water to unsaturated zone and effect of flux boundary conditions due to environmental factors are discussed in here.

2.2.1 Capillary Forces

The mechanism by which water in the saturated zones of fine-grained soils rises above the groundwater table and accelerates into the unsaturated zone is known as the capillarity (Terzaghi, 1942). The upward force that retains the water in the soil pores is called as capillary force. In contrast to the gravitational force, this capillary force acts in the opposite direction. The mechanism of capillary rise of the water to the voids of unsaturated soil is explained using a basic model that depicts the phenomenon of water rising in an air-filled capillary glass tube. *Figure 2.3* represents a cylindrical glass tube of diameter 2r with one end of the tube submerged in water.

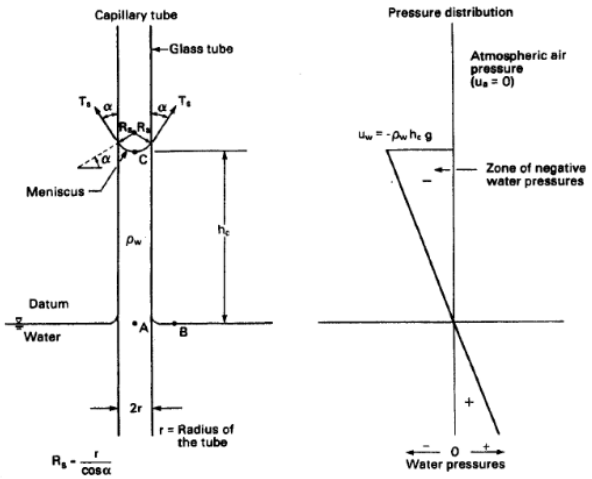

Figure 2.3: Capillary rise of water in a glass tube (Delwyn.G.Fredlund et al., 2012)

The adhesive forces exhibited due to the molecular attraction between the water and the glass tube comprising water results in capillary rise until a equilibrium is established between the gravitational force exerted by the weight of the water $\pi r^2 \gamma_w h_c$ and the upward capillary force F. The surface of the water in the capillary tube assumes a convex curve called as the meniscus. The difference in pressure acting in the water in the capillary tube and the pressure due to air results in surface tension acting around the circumference of meniscus at an angle α_1 . The pressure differential between the air and water below the meniscus is called as capillary pressure p_c. When the air pressure reaches the atmospheric pressure, the capillary pressure becomes negative pore water pressure as shown in equation 2.1 and 2.2

$$p_c = p_{air} - p_{water} \tag{2.1}$$

$$p_c = -p_{water} \tag{2.2}$$

While equating the forces acting along vertical direction, it is evident that the vertical component of surface tension is equivalent to weight of water as illustrated in equation 2.3

$$2\pi r T_s cos\alpha_1 = \pi r^2 h_c \rho_w g \tag{2.3}$$

Thus, the height of capillary rise h_c is represented in the equation 2.4.

$$h_c = \frac{2T_s cos\alpha_1}{R_s \rho_w g} \tag{2.4}$$

In reality, the soil matrix is composed of numerous interconnected voids that functions as capillary tubes of different diameter (Tremblay, 1996). Hence, its difficult to estimate the capillary rise in soil using the equation 2.4. The capillary rise of water in soils is greatly influenced by grain size distribution. Hence, the height of capillary fringe differs based on the soil type, environmental factors such as soil moisture evaporation and precipitation due to varying capillary pore size. The smaller the capillary pore size of the soil (i.e fine grained soils) the larger the capillary rise of water as illustrated in Appendix 1.

2.2.2 Flux boundary conditions

Evaporation at ground level or evapotranspiration by plants are the two mechanisms by which the water from the soil profile is eliminated (Tremblay, 1996). A upward flux of vaporized stream is produced as a result of the evaporation process. On the other hand, when it rains, the water seeps into the ground and creates a downward flux of water. Hence, the varying flux conditions due to environmental factors explains the changes in the pore water pressure in the soil, resulting in soil shrinkage or swelling.

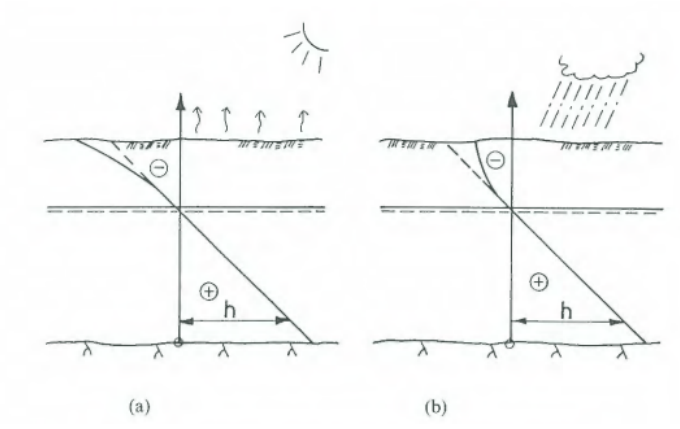

Figure 2.4: a)Pore water pressure under Evaporation b)Pore water pressure under Precipitation (Tremblay, 1996)

In situations where the rate of precipitation surpasses the rate of evaporation in the soil, water is momentarily retained on the ground surface, which causes the negative pore water pressure to drop to zero and increased degree of saturation. Conversely,

excessive soil moisture evaporation from the ground surface may cause the soil to dry out, which raises the negative pore water pressure beyond the expected level at the ground surface and a significant decrease in the degree of saturation as shown in *Figure 2.4*. Hence, the negative pore pressure in a soil profile is significantly affected by the ground water table and flux boundary conditions. Decrease in negative pore water pressure affects the shear strength of the unsaturated soil leading to numerous slope failures.

2.3 Soil suction

In unsaturated soil, the pore water pressure is negative when the air pressure equals the atmospheric pressure (Öberg, 1997). This negative pore water pressure acting in the unsaturated soil zone is commonly referred as soil suction. The pore water pressure is precisely the opposite to the pore water pressure in the saturated zone. Soil suction plays a significant role in determining the mechanical behaviour of unsaturated soil. Matric (u_a -u_w) and osmotic suction (π) are the two components of soil suction, which is referred to as total suction (ψ) when stated in terms of relative humidity. Relative humidity indicates how saturated the soil is in relation to water vapour. The mathematical relationship between the soil suction and its components are illustrated using the equation 2.5.

$$\psi = (u_a - u_w) + \pi \tag{2.5}$$

The difference between the pore-air pressure above and the pore-water pressure below the contractile skin in unsaturated zone is known as matric suction. When the pore-air pressure is precisely equivalent to the atmospheric pressure in the outfield, the total suction results in negative pore water pressure (Delwyn.G.Fredlund et al., 2012). The presence of dissolved salts in pore-water is related with the osmotic suction, which is inversely proportional to relative humidity. The osmotic suction plays a significant role in explaining the mechanical behaviour of both saturated and unsaturated soil. The osmotic suction in soil is insensitive to variations in the water content of the soil, whereas the matric suction in soil is affected by changes in soil moisture caused by environmental factors including infiltration and evaporation at the ground level. Hence, in the majority of geotechnical situations, the osmotic suction is neglected and variations in matric suction are equivalent to variations in total suction. When the water content of the soil is already known, them the soil suction can be calculated. Thus, several empirical equations has been proposed to best fit the relationship between soil suction and water content.

2.4 Soil Water Characteristic Curves (SWCC)

The amount of water that is potentially retained in a soil at equilibrium is illustrated by soil water characteristic curves (SWCC). In other words, the SWCC establishes the relationship between soil suction and water content (Delwyn.G.Fredlund et al., 2012). Multiple variables, including gravimetric water content, volumetric water content, and degree of saturation, can be used to describe the amount of water that

can be retained in the soil. The volumetric water content and degree of saturation are related to volumes while gravimetric water content is related to mass of soil solids as illustrated in Appendix 1.The SWCC has a major influence on the mechanical behaviour of unsaturated soil. It has been found that the curve acts as an illustrative model that provides insights into the distribution of water in voids by employing the capillary model. The SWCC is a hydraulic parameter that is influenced by the mineral composition of soil, grain size distribution, pore-size distribution, permeability coefficient, degree of saturation and matric suction, so the curve can be used to estimate the shear strength of the soil(Hong et al., 2016). Soil gradation has a significant effect on the shape and curvature of the SWCC, so, a well-graded soil will have a smoother soil-water curve than a poorly-graded soil(Öberg, 1997).The SWCC for different soils are shown in *Figure 2.5*, and it is clear that clay measures significantly higher suction than sand at the same water content, indicating that suction is influenced by the grain size distribution(Abed and Vermeer, 2006).

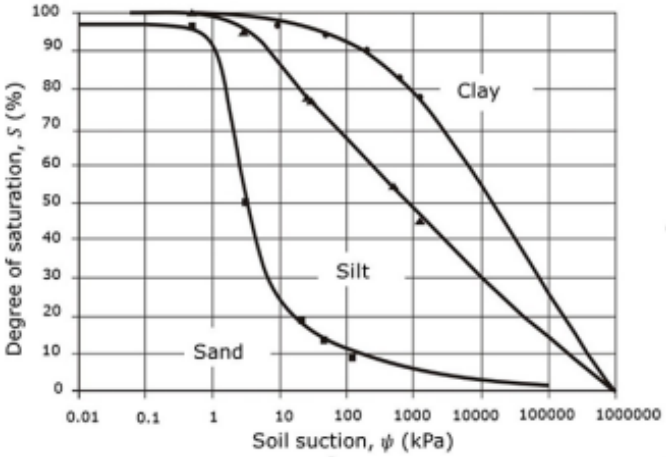

Figure 2.5: SWCC for sand, silt and clay (Kareem and Fadhil, 2018)

The SWCC generally has three different zones of desaturation which includes transition zone, boundary effect zone and residual zone. A typical SWCC stating different zones are presented in *Figure 2.6*. The air-entry value and residual value for suction and water content are the two primary transition points which separates the distinct boundaries on the curve. The air phase is discontinuous while the water phase is continuous in the boundary effect zone. In this zone, pore water is prevented from flowing into the transition zone until the matric suction exceeds the air-entry value, which is indicated by the intersection of two tangent lines that extend from the boundary effect zone and the transition zone, respectively, in the curve. The soil suction at which the air begins to replace the pore water in the voids is called as air-entry value. Suction has a considerable impact on shear strength of the soil when the zone is completely saturated with water. Both the air and the water phases are continuous in the transition zone, and the curve's inflection point indicates the shift in a rapid water content decrease with increased suction to a slower water content decrease as the soil gets closer to residual conditions.The air-phase is continuous and water phase is discontinuous in residual zone (S.K.Vanapalli, 2009).The minimal wa-

ter content that the soil can accumulate under prevailing atmospheric conditions is referred to as residual conditions. The residual conditions of a soil is extremely important to know as they predict the behaviour of unsaturated soil under different meteorological conditions. As the volumetric water content drops, the matric suction increases, leading to a linear increase in shear strength of the soil. Depending on the soil gradation and extend of drainage from soil pores, the shear strength of the unsaturated soil at residual zone can increase, decrease or remain unchanged.

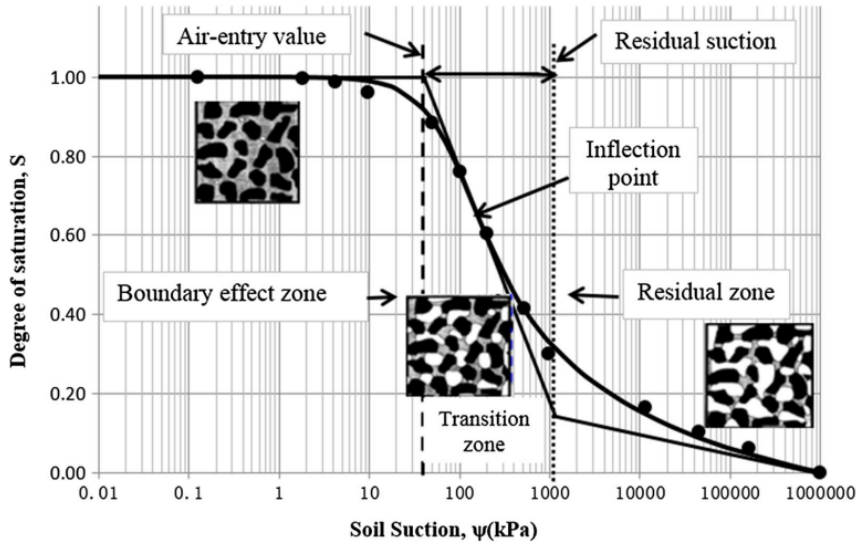

Figure 2.6: Typical SWCC with different zones of desaturation (Zhai et al., 2019)

2.4.1 Hysteresis Effect of SWCC

The water content in the wetting curve will consistently be lower than that in the drying curve for a given matric suction(Yang et al., 2004). This is due to the fact that more water will be retained during the drying period compared to the wetting period. Thus, there will be two distinct SWCCs, depending on whether the soil experiences drying or wetting. This scenario is known as hysteresis. Due to the hysteretic characteristics of the SWCC,it is challenging to calculate a single suction value to the corresponding water content. Hence, its important to compute the soil suction values while considering the hysteresis related with drying and wetting curves (Delwyn.G.Fredlund et al., 2012). The drying curve is called as desorption curve and wetting curve is called as absorption curve. The unique relationship between the matric suction and water contents as a hysteresis loop of SWCC is presented in *Figure 2.7*. The drying curve is measured in laboratory while the wetting curve is either measured at laboratory or using the empirical recommendations. Some of the observations made from the *Figure 2.7* include:

- During several drying and wetting cycles, the SWCC hysteresis loop seems to be repeatable.
- When soil is desaturated beyond residual conditions, the drying curve's slope

seems to lie parallel to the wetting curve.

- Some of the air remain trapped in the pores even after the soil has saturated.
- Both the drying and wetting curves have inflection point which is used to define the lateral shift between desorption and adsorption in unsaturated soil.

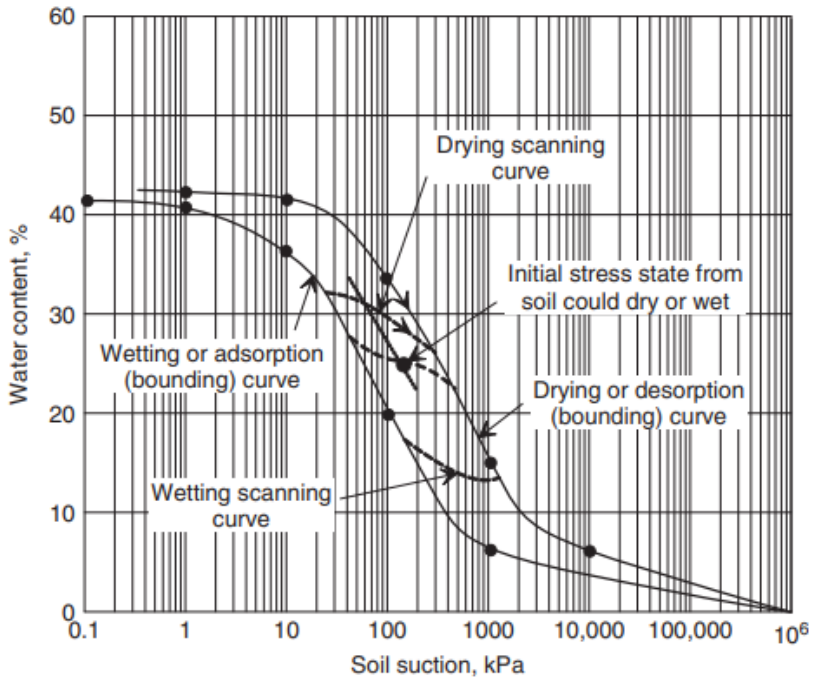

Figure 2.7: Hysteresis loop of SWCC (Delwyn.G.Fredlund et al., 2012)

From the *Figure 2.7* it is evident that air occupies the large voids of the soil when the soil is desaturated (Öberg, 1997). The matric suction along the drying curve that facilitates air entry into the pores is referred to as air-entry or bubbling pressure. Conversely, during the wetting period, water infiltrates the pores, saturating the soil and increasing its water content. The hysteresis loop is therefore continued until there is no noticeable volume change in the soil. This mechanism contributes to the hysteresis phenomena seen in soil-water interactions by highlighting the dynamic relationship between pore air, pore water, and soil moisture content.

2.5 Empirical Equations to estimate SWCC

According to researchers, soil-water characteristic curve (SWCC) has been used to calculate a number of unsaturated soil properties, including coefficient of consolidation, shear strength, and coefficient of permeability (Chin et al., 2010). Numerous scholars have proposed a range of empirical equations to determine the relationship between soil suction values and water content in order to accurately fit the SWCC. Most of these equations are effective for a particular type of soil, and finding an equation that is effective for all soil types has been a problem for several researchers in past decades (E.C.Leong, 1997). These equations were developed based on the

sigmoidal shape of the curve. The curve fitting equations are estimated either from direct estimation of water content and matric suction during laboratory testing, or indirect estimation using grain size distribution, which provides insight into the soil pore's ability to hold water (Huvaj et al., 2012).

In the early 1950s, Gardner introduced an empirical model aimed at describing the permeability of unsaturated soil (Delwyn.G.Fredlund et al., 2012). Subsequently, the equations were rearranged to estimate soil suction. Later in 1960s, Brooks and Corey proposed a macroscopic model that divided the Soil-Water Characteristic Curve (SWCC) into two zones. This division resulted in obtaining two soil suction values: one less than, and one greater than the air-entry value. In 1980s, Van Genuchten proposed an equation with three curve-fitting parameters that offered flexibility in fitting a variety of soil types. The resulting equation could accurately calculate the soil suction between air-entry and residual conditions and more accurately represented the sigmoidal shape of typical curves. This enhances stability while optimising parameters and enables the hydraulic conductivity function to be solved in closed form. Later, Fredlund and Xing (1994) proposed a formula by implementing a correction factor such that it could be used to the soil beyond its residual condition, all the way to complete desaturation. At high suction values, the correction factor makes the water content zero. Scientists then made several efforts to predict the parameters for unsaturated soil using these two well-known equations as a foundation.

Z.Zhang et al., 2013 proposed a model by incorporating the changes in void ratio to the SWCC model. The model was based on Van-Genuchten model. Pham and G.Fredlund, 2003 dicussed about the need for a developing empirical model that establishes a SWCC by considering hysteretic effect. The model was developed based on Fredlund equation and the author claimed that the curve fitting equation is best suitable to low swelling soil. Indeed, numerous statistical models have been employed to develop Soil-Water Characteristic Curves (SWCCs) based on various factors such as grain-size distribution, pore-size distribution, and index properties of the soil. Chin et al., 2010 suggested a simple approach that uses the Fredlund equation and index properties of soil to estimate the SWCC for both coarse- and fine-grained soil. The investigation was conducted by replacing the particle size at the 60th percentile (D_{60}) with a variable for each of the two types of soil. The results indicated that the use of Fredlund and Xing (1994) equation has established a SWCC that performs well even at low suction range and the soil suction was always set to 1 kPa at zero volumetric water content upon incorporation of correction factor. Thus, when the results are compared with other approaches, they outperformed the existing one-point approaches. E.C.Leong, 1997 investigated frequently used empirical equations proposed over the years to describe the SWCC and to determine the unsaturated soil parameters. The study aimed to identify an equation that could effectively model SWCCs for all soil types. The empirical equations that provide a sigmoidal curve and the equations that do not reflect a sigmoidal SWCC were identified. When comparing the curve fitting parameters and SWCCs obtained using the equations proposed by Gardner (1958), Van Genuchten (1980), and Fredlund and Xing (1994),

it became evident that the equation recommended by Fredlund provided the most accurate fit of SWCCs compared to the other equations.

Azmi et al., 2016 focuses on validating the SWCC models developed using Van-Genuchten and Fredlund and Xing for mining sand. Laborartory tests have been conducted on to determine the physical properties of the soil such as index properties, water content, specific gravity and grain size distribution. Additionally, the suction and corresponding water content of the soil samples were determined using the pressure plate method. Then, using the matric suction and water content data, the three curve fitting parameters were obtained. The experimental results were then compared with the predictions of the mathematical equations. It was observed that both the Van Genuchten and Fredlund and Xing models have a satisfactory match for the whole range of experimental data. These models also showed almost exact SWCC predictions, demonstrating their accuracy in describing the soil-water connection in mining sand.

While several empirical models such as Gardner (1958), Brooks and Corey (1964), Van Genuchten (1980), and Fredlund and Xing (1994) exist to characterize the mechanical behavior of unsaturated soil using Soil-Water Characteristic Curves (SWCC), this thesis specifically delves into examining the numerical response of silty slopes under flux boundary conditions using the Van Genuchten model (1980). Empirical equations with parameters for the remaining approaches are detailed in Appendix A

2.6 Van-Genuchten model (VG)

Van-Genuchten (1980) proposed a three parameter equation to establish a relationship between soil suction and volumetric water content of unsaturated soil in the form of sigmoidal curves (Delwyn.G.Fredlund et al., 2012). The SWCC can be defined when the three curve fitting parameters and saturated water content (w_s) are known. The parameter a in the SWCC represents a soil suction value that is slightly greater than the air-entry value. The parameter n governs the rate at which soil desaturation occurs as suction surpasses the air-entry value, thereby influencing the slope of the water retention curve. The parameter n is related to grain-size distribution. The parameter m offers enhanced flexibility across a broad spectrum of suction values, ensuring a more precise capture of the sigmoidal curve and inflection point. Thus, the model resulted in smooth transitioning in curves when suction approaches the air-entry and residual conditions in the curves. The VG model empirical equation is presented in the form of water content at corresponding soil suction w(ψ) as shown in the equation 2.6:

$$w(\psi) = \frac{w_s}{[1 + (a\psi)^n]^m} \tag{2.6}$$

The VG equation can be reformulated to determine soil suction ψ based on water content as shown in equation 2.7:

$$\psi = \frac{1}{a}\left[\left(\frac{w_s}{w}\right)^{\frac{1}{m}} - 1\right]^{\frac{1}{n}} \tag{2.7}$$

Initially, the VG model was represented by three curve fitting parameters but later empirical equation was modified into two parameter model (Delwyn.G.Fredlund et al., 2012). This modification offered improved accuracy when anticipating the cure fitting parameters and facilitated the estimation of permeability using SWCC. The empirical form of VG model offers a stable relationship between parameter n and m as shown in equation 2.8:

$$m = \frac{n-1}{n} \tag{2.8}$$

The water content at saturation, w(ψ), is often referred to as the normalized water content, denoted by θ_n. With an increase in matric suction and a subsequent decrease in water content, the soil experiences minimal to no volume changes. In this context, the normalized water content is equivalent to the effective saturation (Delwyn.G.Fredlund et al., 2012). The normalized water content θ_n or effective saturation S_e can be calculated using the relationship between residual water content θ_r and saturated water content θ_s as illustrated in equation 2.9:

$$S_e = \theta_n = \frac{\theta - \theta_r}{\theta_s - \theta_r} \tag{2.9}$$

The coefficient of permeability of unsaturated soil relies on the volumetric water content and soil suction (Delwyn.G.Fredlund et al., 2012). Thus, the permeability is expressed in terms of permeability coefficient and soil suction. As mentioned before, the relative coefficient of permeability can be calculated using the VG model as expressed in equation 2.10 (Lu and J.Likos, 2004).

$$K_r(\psi) = \frac{[1 - (a\psi)^{n-1}[1 + (a\psi)^n]^{-m}]^2}{[1 + (a\psi)^n]^{\frac{m}{2}}} \tag{2.10}$$

The coefficient of permeability $K_w(\psi)$ at corresponding soil suction is the product of saturated K_s and relative $K_r(\psi)$ coefficient of permeability as expressed in equation 2.11:

$$K_w(\psi) = K_s K_r(\psi) \tag{2.11}$$

2.7 Stress State variables

State variables can be described as the ability to define the physical behaviour of a given material, such as unsaturated soil in the present scenario (Delwyn.G.Fredlund et al., 2012). The identification of state variables linked to stress state has played a pivotal role in understanding material behavior. Similarly, the recognition of effective stress variables related to unsaturated soil has catalyzed advancements in the field of unsaturated soil mechanics. Therefore, the key state variables for unsaturated soil should depict changes in volume, shear strength, distortion and deformation. It is also necessary to draw attention to state variables other than stress related variables such as deformation, temperature and time, as they play a vital role in describing the mechanical behaviour of unsaturated soil. For instance, unsaturated soil typically appears close to the ground surface where it is exposed to varying environmental conditions such as evaporation and transpiration on regular intervals. The varying temperatures during evaporation and transpiration process causes major changes to the mechanical properties of the soil and controls the behaviour of unsaturated soil. Hence, temperature becomes one of the key state variable to be focused on.

2.7.1 Terzaghi's effective stress variable

The effective stress variable is used to predict the soil behaviour and is relevant to all soil types which includes sand, silt and clay (Delwyn.G.Fredlund et al., 2012). The key state variables that depicts the volumetric strain and shear strength properties are controlled by the effective stress variables. In 1936, Terzaghi formulated effective stress principle that controls the behaviour of saturated soil. Effective stress is the difference between the total stress and pore water pressure. According to Terzaghi, stresses exerted on a soil mass at any given point can be calculated from the principal stresses σ_1, σ_2 and σ_3 acting at that particular point. This total principal stresses acting in three different directions changes into two distinct components when the voids of the soil become saturated with water under a stress u_w. The stress u_w acts with equal intensity in both water and solid phases in all three directions. This stress is referred to as pore water pressure. Thus, Terzaghi's effective stress variables for saturated soil can be expressed in two theories (J.B.Burland, 1962) :

- The measurable effects experienced by soil from stress variations, including compression, shear resistance, and distortion, are attributed to changes in effective stress, determined by principal stress σ_1, σ_2 and σ_3.

- Effective stress σ' is a stress variable used to understand the mechanical behaviour of saturated soils. Effective stress is defined as the difference between total stress applied on the soil (σ) and the pore water pressure (u_w) as represented in equation 2.12: .

$$\sigma' = \sigma - u_w \tag{2.12}$$

$$\begin{bmatrix} \sigma_x - u_w & \tau_{yx} & \tau_{zx} \\ \tau_{xy} & \sigma_y - u_w & \tau_{zy} \\ \tau_{xz} & \tau_{yz} & \sigma_z - u_w \end{bmatrix} \tag{2.13}$$

Skempton (1960) has validated the efficacy of the effective stress variable $\sigma - u_w$, affirming its adequacy in describing the behavior of saturated soils (J.B.Burland, 1962). The stress state variables of saturated soil can be expressed as a matrix incorporating effective stress variables in all three Cartesian coordinate directions, as depicted in the equation 2.13. This matrix representation offers enhanced clarity, revealing that any changes in either the total stress applied or pore water pressure can significantly impact the effective stress of the soil, thereby influencing its equilibrium state (Delwyn.G.Fredlund et al., 2012). Several attempts have been made by scientists to extend the classical effective stress theory of fully saturated soil to partly saturated soil. However, this extension required modifications to the equations to ensure their validity for the behavior of unsaturated soil. This phenomenon occurs because, as the volumetric water content decreases, air tends to replace the pore water in unsaturated soil. Consequently, suction increases along the drying curve, making the effective stress equation of saturated soil no longer applicable for partly saturated soil.

2.7.2 Bishop's effective stress variable

Biot (1941) established a consolidation theory for unsaturated soil, devising a constitutive equation that correlates stress and strain using two distinct stress state variables such as effective stress variable $(\sigma - u_w)$ and pore water pressure (u_w) (Delwyn.G.Fredlund et al., 2012). While attempting to describe the behaviour of unsaturated soil using effective stress variables formulated by Terzaghi, Biot recognized the necessity to distinguishing between the effects of total stress variations and changes in pore water pressure as two separate variables. Later in 1959, Bishop reassessed the existing effective stress equation for partly saturated soil and found that any changes in matric suction $(u_a - u_w)$ did not induce the same changes in soil behaviour, but contributed the same changes to the net normal stress $(\sigma - u_a)$. Bishop (1959) proposed a effective stress equation for unsaturated soil correlating matric suction to net normal stress by incorporating a soil parameter χ as defined in equation 2.15

$$\sigma' = (\sigma - u_a) + \chi(u_a - u_w) \tag{2.14}$$

The soil parameter χ in the equation is associated with the degree of saturation of the soil, which typically varies between 0 and 1 (Delwyn.G.Fredlund et al., 2012). This parameter χ is derived under the assumption that soil behavior can be adequately described using a single effective stress variable. Additionally, it is obtained by establishing correlations between the behavior of unsaturated soil and the behavior of saturated soil. Further, the stress state variables for the unsaturated soil is expressed in terms of two independent stress tensors acting in all the three Cartesian

coordinate directions. The unsaturated soil generally has a air-water interface, hence the stress state variables for contractile skin is also accounted. The two independent stress tensors for unsaturated soil can be represented as in equation 2.15 and 2.16

$$\begin{bmatrix} \sigma_x - u_w & \tau_{yx} & \tau_{zx} \\ \tau_{xy} & \sigma_y - u_w & \tau_{zy} \\ \tau_{xz} & \tau_{yz} & \sigma_z - u_w \end{bmatrix} \tag{2.15}$$

$$\begin{bmatrix} u_a - u_w & 0 & 0 \\ 0 & u_a - u_w & 0 \\ 0 & 0 & u_a - u_w \end{bmatrix} \tag{2.16}$$

From the matrix, it becomes apparent that as unsaturated soil transitions to a saturated state, the degree of saturation reaches (Delwyn.G.Fredlund et al., 2012). Consequently, the pore water pressure increases until it matches the pore air pressure, effectively reducing the matric suction value to zero in both the stress state tensors. This condition leads to the complete elimination of the second stress tensor in unsaturated soil, as all its values become zero.

2.7.3 Limitations of Terzaghi's effective stress variable

The principle of effective stress is a fundamental concept in soil mechanics that attributes the mechanical behavior of soil to the effective stress acting on the soil skeleton (Delwyn.G.Fredlund et al., 2012). Saturated soil is a two-phase system which considers the interaction between solid particles and pore water. However, in unsaturated soil, the presence of both water and air in the pore spaces introduces additional complexities. The negative pore water pressure induced by the presence of air bubbles within the pore spaces of unsaturated soil significantly influences the effective stress. Consequently, the application of Terzaghi's effective stress principle, originally devised for saturated soil, encounters limitations when extended to unsaturated soil. This limitation becomes apparent through a comparative analysis using Terzaghi and Bishop formulations.

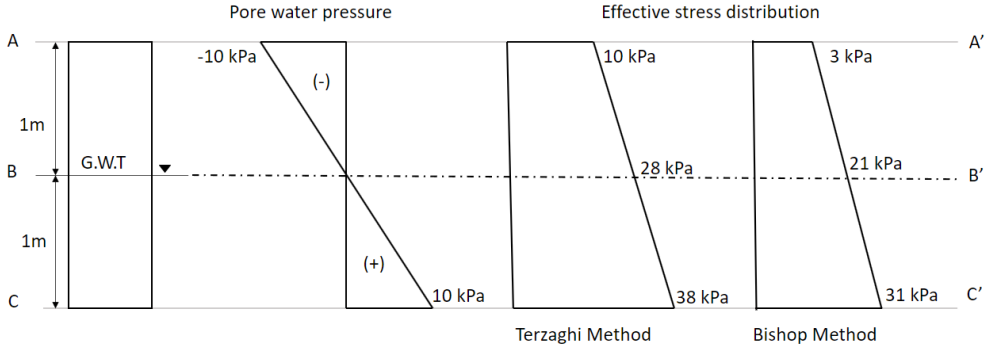

Figure 2.8: Effective stress distribution using Terzaghi and Bishop Method

To illustrate, let's consider a silt soil sample with a height of 2 meters, where the water table lies 1 meter below the soil surface. The soil below the water table is fully saturated. Assuming the unit weight of water γ_w as 10 kPa, and the dry γ_{unsat} and saturated unit weights γ_{sat} of the silt as 18 kPa and 20 kPa respectively, the effective stress is computed using both methods. The stress diagram is presented in the *Figure 2.8*. The calculated effective stress and pore water pressure values are outlined in the Appendix A. The *figure 2.8* clearly demonstrates that when employing Terzaghi's effective stress variables for unsaturated soil, the resulting effective stress values are not conservative; instead, they yield magnified values.

2.8 Slope stability

Slope stability analysis is the investigation of natural geological formations that exists or man-made slopes to identify potential failure mechanisms or triggering factors (VNS.Murthy, 2003). Climatic and geological conditions have historically played pivotal roles in causing slope failures, often leading to catastrophic loss of life and property. Slope stability analysis refers to the optimal design of slopes by evaluating the resisting and driving forces acting upon them. The stability of any slope is dependent on its ability to balance resisting forces owing to its self-weight and external driving forces without causing sliding or deformation. While slope stability is undeniably a crucial consideration in engineering design, many geotechnical engineers encounter significant challenges related to slope instability or failure. Slope instability occurs when the external forces acting on a soil slope exceed the resisting forces, disrupting equilibrium (Ullah et al., 2020). This can result from a multitude of factors, both internal and external, that influence the shear strength of the soil. Internal factors such as soil properties such as shear strength and cohesion, particle size distribution, slope geometry, soil weight and distribution, surcharge loads, water content and fluctuations in groundwater levels can contribute to increased stress and subsequent soil failure (Gebreyohannes et al., 2024). Conversely, external factors such as weathering, cyclic loads, heavy rainfall, vegetation, geological conditions and human activities that disrupt the equilibrium also play significant roles in exacerbating slope instability. In stability analysis, it's often assumed that the development of shear strength from negative pore water pressure above the groundwater table is negligible (Delwyn.G.Fredlund et al., 2012). Additionally, conventional slope stability investigations typically treat saturated and unsaturated soil as having the same total weight, which affects the analysis results. Usually, negative pore water pressure is ignored by setting it to zero, and slope stability is assessed solely based on shear strength influenced by positive pore water pressure in saturated soil. However, recent research suggests that the emergence of negative pore water pressure or matric suction in unsaturated soil can increase the shear strength of the slope. Therefore, this study aims to investigate the impact of negative pore water pressure on slope stability and factor of safety calculations by providing insights into more accurate and robust slope stability assessments in geotechnical engineering practice.

Instability in soil slope occurs from various internal and external factors, resulting in slope movement (i.e.sliding) triggered by a sudden or gradual decline in shear strength of the soil (R.F.Craig, 1983). Common types of slips anticipated in soil slopes include rotational, translational, or compound slips as shown in *figure 2.9*. Rotational slips may feature a failure surface shaped as either a circular arc or a non-circular slips. Circular slips typically occur in homogeneous soil conditions, whereas non-circular slips are characteristic of non-homogeneous soil conditions. Translational and compound slips, on the other hand, occur when adjacent soil strata of varying strengths influence the failure. Translational slips involve a failure surface that is planar and parallel to the slope, often occurring when adjacent soil strata are situated at shallower depths beneath the slope surface. Compound slips exhibit a failure surface that is curved at the ends and planar at the center, usually occurring when adjacent soil layers are found at greater depths.

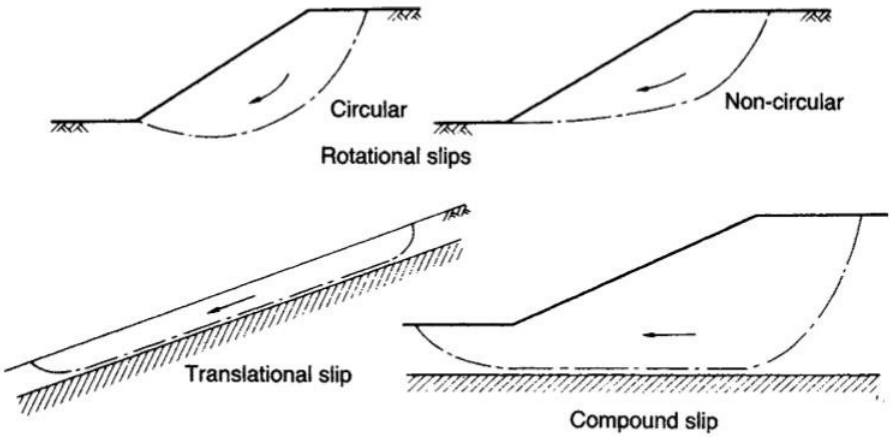

Figure 2.9: Slope failure mechanism (R.F.Craig, 1983)

Typically, slope stability is quantified using a scalar unit called as factor of safety (FOS) (Duncan et al., 2014). Changes in the loads exerted on the slope and variations in shear strength significantly affect the factor of safety. Consequently, depending on the soil conditions, the FOS for slope stability may either increase or decrease. The FOS in stability calculations can take two forms factor of safety due to cohesion and friction angle or factor of safety related to shear strength(VNS.Murthy, 2003). The factor of safety is typically defined as the ratio of shear strength to shear stress in soil as in equation 2.17

$$F = \frac{S}{\tau} \tag{2.17}$$

To maintain slope stability, the shear strength needed along the critical failure plane is calculated and compared with the available shear stress (Duncan et al., 2014). The equilibrium shear stress, calculated by dividing the available shear strength by the factor of safety, signifies how much the available shear strength must be reduced to balance with the required shear stress for slope stability. This method of assessing slope stability is commonly referred to as the limit equilibrium method. In limit

equilibrium method the shear strength of the soil is expressed by utilising the Mohr-Coulomb equation. The shear stresses can either be expressed as total stress or effective stress as shown in equation 2.18 and 2.19.

$$\tau = \frac{c_d + \sigma \, tan \, \phi_d}{F} \tag{2.18}$$

$$\tau = \frac{c' + (\sigma - u) tan \, \phi'}{F} \tag{2.19}$$

Shear strength is expressed in terms of total stress during undrained-unconsolidated tests on saturated clays, while effective stress is utilized for drained analysis, where shear strengths represent drained shear strengths (Janbu, 1973). When the FOS equals 1, it indicates that the slope is in a delicate equilibrium between stability and instability (Duncan et al., 2014). This equilibrium signifies that the forces maintaining stability are equal to those potentially destabilizing the slope. Therefore, a FOS below 1 signifies instability, whereas values exceeding 1 indicate stable slope. Therefore, the FOS plays a crucial role in addressing uncertainty and the reliability of factors involved in the analysis, such as soil strength parameters, pore pressure distribution, and stratigraphy (Abramson et al., 2002). Additionally, the FOS can be calculated using two alternative methods besides the limit equilibrium method, as detailed in the Appendix A. However, it is important to note that the factor of safety values obtained from these three different methods may not be identical for soils c-ϕ whose shear strength properties are expressed in terms of cohesion and friction angle.

During numerical modeling and slope stability analysis, the computation of the factor of safety can vary based on the soil model and software tool utilized (Bentley, 2020). In PLAXIS, for instance, it's advised to avoid using the K_0 procedure for non-horizontal surfaces, such as sloping ground. Instead, employing a gravity loading method with an appropriate material model is recommended to establish the initial stress conditions. For gravity loading under drained condition, either the Mohr-Coulomb or Hardening Soil model is suggested. Since the factor of safety is based on the Mohr-Coulomb model, it is recommended to employ this model in PLAXIS for stability analysis. In PLAXIS, stability analysis for determining the factor of safety utilizes c-ϕ method. Here, shear strength and tensile parameters are systematically reduced until failure is reached. The resulting factor of safety, calculated through an equation 2.20 is represented by a total multiplier $\sum M_{\text{sf}}$.

$$\sum M_{\text{sf}} = \frac{tan \, \phi_{input}}{tan \, \phi_{reduced}} = \frac{c_{input}}{c_{reduced}} = \frac{Tensile \, strength_{\, input}}{Tensile \, strength_{\, reduced}} \tag{2.20}$$

2.9 Mohr-Coulomb Model

Mohr- Coulomb is a elastic-perfectly plastic model which is considered as a first - order model because its been widely used by geotechnical engineers to model the soil behaviour (Ti et al., 2017). The model adheres to a perfectly plastic theory, hence neglecting any possibility of recovery after surpassing a specific strain threshold.

In general, a method to conceptualize soil behavior is by regarding it as exhibiting elastic behavior until it surpasses a yield point, after which it undergoes plastic deformation until it reaches failure (Briaud, 2023). Beyond the yield point the soil can exhibit strain hardening, strain softening or perfectly plastic behaviour. The yield criteria and failure criteria are same when the material is perfectly plastic beyond the yield point. While the criteria are not same when the material exhibits strain hardening or strain softening. In non-linear theory, the strains are divided into an elastic and plastic component to distinguish the behaviour of materials under different stress conditions. The elastic strains are recoverable while the plastic strains are unrecoverable. In a plastic theory, there exits three important components namely, yield function, plastic potential and hardening or softening rule. The yield function and associated yield criteria provides stresses in combinations that results in soil yielding. The plastic potential determines the direction of plastic strain increments through a flow rule, while the magnitude is dictated by the hardening or softening rule. When the plastic potential matches the yield function, the flow rule is considered associated; when the functions differ, the flow rule is termed non-associated. The stress combinations determined by the yield function and the corresponding criteria can be elucidated using the Mohr-Coulomb failure criteria. According to Mohr-Coulomb failure criteria the when the mobilised shear stress at any plane becomes equal to the shear strength, the soil mass experiences the yielding or failure as shown in *figure 2.10*. The Mohr-Coulomb criteria can be formulated using strength parameters c' and ϕ' as in equation 2.21, and it can alternatively be reformulated in terms of major and minor principal stresses in equation 2.22. In Mohr-Coulomb model, the flow rule is exhibited using the dilatancy angle.

$$\tau_f = c' - \sigma' \tan \phi' \tag{2.21}$$

$$\sigma'_1 - \sigma'_3 - 2c' cos\phi' = (\sigma'_1 + \sigma'_3)\, sin\phi' \tag{2.22}$$

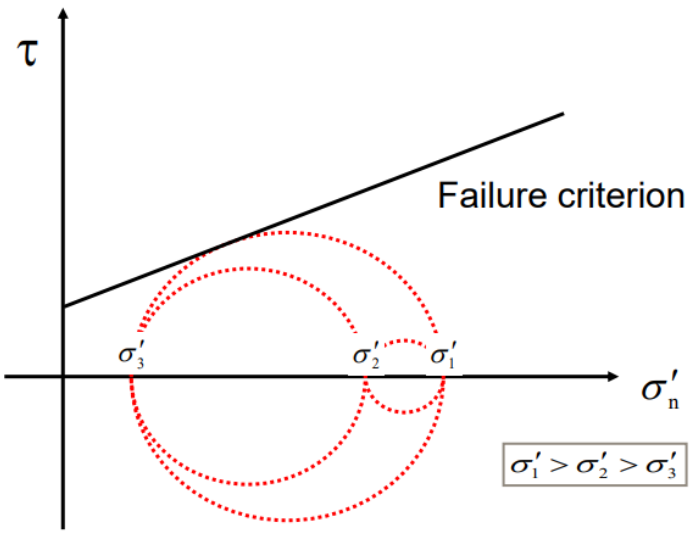

Figure 2.10: Mohr-Coulomb failure criteria (Briaud, 2023)

The Mohr-Coulomb failure surface in three-dimensional stress space is depicted in the *figure 2.11* corners of the hexagon can pose computational challenges (Briaud, 2023). Some numerical modeling tools encounter difficulties in implementing the Mohr-Coulomb model because of the intersection of two yield surfaces. However, PLAXIS facilitates a seamless implementation of the model by enabling a sharp transition from one yield surface to another (Bentley, 2015).

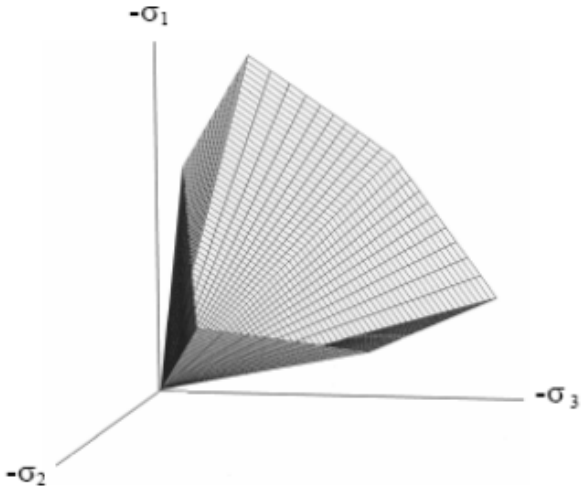

Figure 2.11: Mohr-Coulomb yield surface (Ti et al., 2017)

2.10 Finite element Analysis

Over time, engineers have devised various conventional techniques to address geotechnical challenges that they encountered such as excavations, foundation construction, embankments, retaining walls and tunnels (N.Radhakrishnan and Lymon.C.Reese, 1970). These non-numerical or conventional methods are often faster and cost-effective, relying on limited assumptions such as treating soil behavior as linearly elastic, despite its actual non-linear elastoplastic nature, and assuming uniform ground conditions (Lees, 2016). Despite making several assumptions and yielding conservative outcomes, these methods generally provide satisfactory designs without incurring potential economic losses. However, it's important to note that, conventional methods are suitable for addressing many geotechnical problems but they may not always deliver precise results or accurately depict real-time conditions.

On the contrary, numerical modeling has demonstrated effectiveness in addressing both simple and complex geotechnical challenges (Lees, 2016). However, the approach is time consuming and demands more resources when compared to the conventional methods. Thus, it's crucial to meticulously choose the method to ensure its justification. Indeed, various numerical methods are employed in engineering for solving differential equations such as Finite Difference Method (FDM), Finite Element Method (FEM), Discrete Element Method (DEM) and Material Point Method (MPM) (Brandell and Sellden, 2022). Among these methods, the FEM stands out as one of the most widely used techniques, particularly in fields like structural analysis

and geotechnical engineering .The introduction of Finite Element Method (FEM) in numerical modeling of geotechnical problems has indeed brought about a significant improvement in the precision of results obtained. FEM is a computational approach utilized to tackle initial value problems in continuum mechanics and boundary value challenges (N.Radhakrishnan and Lymon.C.Reese, 1970). With the advent of high-speed computers, the utilization and advancement of FEM have seen significant acceleration across various domains. FEM exhibits the capability to handle intricate and practical scenarios involving diverse material properties such as isotropic or anisotropic behavior, along with linear or nonlinear material responses, as well as complex boundary conditions and structural configurations. FEM empowers engineers to address complex situations by discretizing the structure into smaller, more manageable elements interconnected through nodes. These elements are subdivided either into areas or volumes depending on whether the structure is two-dimensional or three-dimensional, respectively. Typically, FEM is considered over conventional methods when dealing with geotechnical projects such as excavations, embankments, slopes, tunnels etc characterized by intricate geometries and hydraulic conditions (Lees, 2016). While, employing constitutive models like hardening or soft soil models, which entail complex boundary conditions. FEM becomes essential for studying soil-structure interaction under complex loads, analyzing the effects of consolidation and creep, examining the impact of construction sequencing in various construction methods, and conducting back-analysis of structural behavior Girijavallabhan and Reese, 1968. pioneered the use of FEM in addressing problems involving soil. They conducted laboratory experiments to examine the load-deformation characteristics of a vertical plate when laterally displaced against sand. The findings were then compared with FEM results, revealing a close resemblance in deformation patterns.

2.10.1 PLAXIS 2D

PLAXIS 2D is an advanced software tool designed for two-dimensional numerical analysis (Bentley, 2020). Using the finite element method, it effectively models a variety of complex geotechnical challenges, including deformation, stability, settlement, consolidation, and flow analysis. The software is highly esteemed for its exceptional performance and effectiveness in stimulating real-world scenarios. It achieves this by offering the flexibility to model situations using either a plane strain or an axisymmetric model. The soil layers can be represented using either 6-noded or 15-noded triangular elements. The 6-noded elements offer decent accuracy and provide satisfactory results in deformation analysis. They employ second-order interpolation for displacements, utilizing three Gauss points. On the other hand, the 15-noded triangular elements are highly accurate, especially for complex geotechnical problems. They offer fourth-order interpolation for displacements and utilize twelve Gauss points, resulting in high-quality results

The program is segmented into four main domains: Input, Calculations, Output, and Curve Generator (Gunduz, Lund University). The software employs a user-friendly graphical interface, enabling users to generate the model's geometry within the input domain. The boreholes serves the function of creating and defining the

different soil layers within the geometry or soil profile (Bentley, 2020). They also enables the user to assign various geotechnical properties of the soil such as soil type, strength parameters and water head establishing the initial conditions. Material properties for each soil type can be defined and managed within the material sets tab in PLAXIS software. This includes specifying details such as the soil type, material behavior under drained or undrained conditions, strength parameters, stiffness, and groundwater flow parameters such as permeability. This comprehensive data allows users to accurately characterize the behavior of different soils and ensuring reliable simulations of soil-structure interaction.

Subsequently, the modelled geometry is transformed into a finite element mesh based on vertical cross-section of the model (Bentley, 2020). The mesh is typically regenerated every time any modifications are made to the geometry. The process of mesh generation depends on a resilient triangulation procedure and its vital to have fine mesh for accurate results. However, excessive mesh refinement can also prolong calculation times significantly. Certainly, in regions where significant stress concentrations or deformations are anticipated, employing a finer mesh is advisable as it yields greater accuracy compared to coarser mesh elements. Conversely, in situations where localized refinements are necessary, such as at edges or corners of the geometry, the coarseness factor can be adjusted to reduce the relative element size in relation to the target element size.

In PLAXIS 2D, total stress is divided into effective stress and active pore pressure during effective stress analysis (Bentley, 2020). Active pore pressure results from the multiplication of effective saturation and pore water pressure. An essential feature of the PLAXIS tool is its capability to conduct analysis for saturated soil beneath the phreatic level, as well as for unsaturated soil above the phreatic level. Additionally, pore water pressure is categorized into steady-state and excess pore water pressure. The pore water pressure that arises under steady-state conditions is termed as steady-state pore pressure, whereas excess pore pressure emerges due to variations in stress induced by external loading, unloading, consolidation, or variations in groundwater flow. The Phases window is where steady-state pore pressures are specified using the pore pressure calculation type. However, in analyses like fully coupled flow-deformation analysis, it is not feasible to select the pore pressure calculation type. In such cases, the total pore pressure is computed instead.

FE analysis can be conducted by breaking down the construction sequence into various phases (Bentley, 2020). Regardless of the calculation type, stage construction involves creating an initial phase followed by subsequent phases relevant to the preferred analysis type. The initial stress condition of the soil can be established by selecting an appropriate calculation method, either K_0 procedure or gravity loading. Typically, slope stability analysis is conducted using the Safety analysis phase as the calculation type, followed by the initial phase. This sequence often leads to a failure state and provides the factor of safety. Once the phases are created, the groundwater flow boundary conditions such as seepage, closed, inflow or infiltration is assigned to the geometry before performing the calculation. Once all the steps have been

assigned, the analysis is performed by initiating the calculation. Throughout the calculation process, the information about each phase that has been is computed in specified in the window that appears on the screen.This window displays details such as load-displacement curves, the number of completed steps, plastic points, and global errors. Once the analysis is completed, the results can be accessed in a separate Output tab. Here, users can examine displacements, failure surfaces, suction and saturation levels, stress distributions, and pore water pressure distributions. Additionally, separate curves can be generated for each result type using a previously selected node on the geometry.

2.10.2 PLAXIS - Remote Scripting using Python

One of the key advantages of using PLAXIS software for finite element analysis is its ability to utilize Python scripting for designing and analyzing models (Bentley, 2020). PLAXIS provides a Python - Application Programming Interface (API) that enables users to customize the software to meet their specific requirements, facilitates the performance of advanced analyses and allows users to execute multiple tasks simultaneously. This kind of method saves time when multiple calculations for similar applications are performed. Users can perform remote Python scripting by converting command line input and output into commands for Python scripts. Both the command runner in PLAXIS and Python remote scripting enable users to utilize commands not exposed by the User-Interface (UI) tools. They also allow for storing and executing macros. Each PLAXIS command is identified by its name, target, and sometimes a parameter. The process of converting command line input into equivalent Python code in PLAXIS is illustrated in the *figure 2.12* and *figure 2.13*.

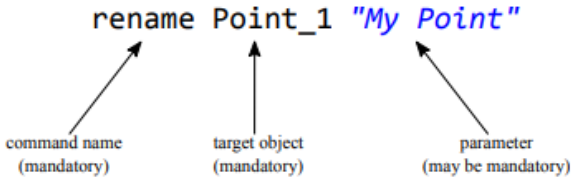

Figure 2.12: Input command line in PLAXIS (Bentley, 2020)

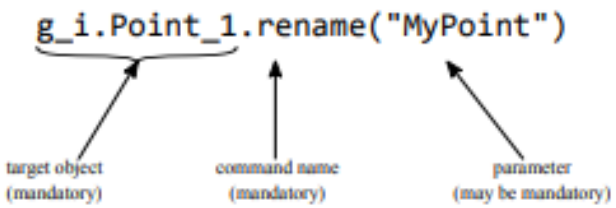

Figure 2.13: Python script for PLAXIS (Bentley, 2020)

To start with Python remote scripting, configuring the server is the first step. Under the <Expert> tab, select "Configure Remote scripting Server" to set up the Python

scripts. This action opens a tab where you can set a password and configure the available port for remote users and the server is established by selecting the start server icon as shown in *figure 2.14*.Typically, a default password is generated, but users have the option to change it.

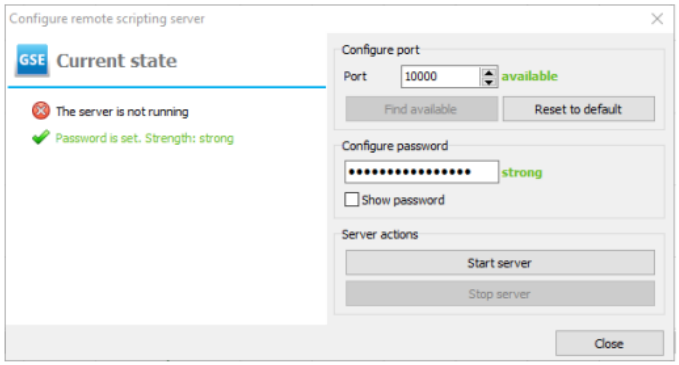

Figure 2.14: Configuring the remote scripting server in PLAXIS (Bentley, 2020)

After configuring the server and setting the password, the user can open and run the Python script by importing the scripting library. The Python script can connect to the PLAXIS server by importing the same port number and password derived from the configuration window.

Further, number of inputs are coded in python to perform the analysis in PLAXIS. Python scripting enables users to automate various tasks in PLAXIS, allowing them to perform all the steps available in the software. Users can create scripts to set soil contours, define coordinates for model geometry, and specify soil layers and their material properties using Python code. Additionally, based on the type of analysis being performed such as plastic, consolidation, safety, or fully-coupled deformation analysis specific scripts are generated to set groundwater boundary conditions for the geometry. Since, the thesis aims to investigate the effect of SWCC on unsaturated soil, a fully-coupled deformation analysis is being carried out. The flowchart depicting the remote scripting process is represented in *figure 2.15*.

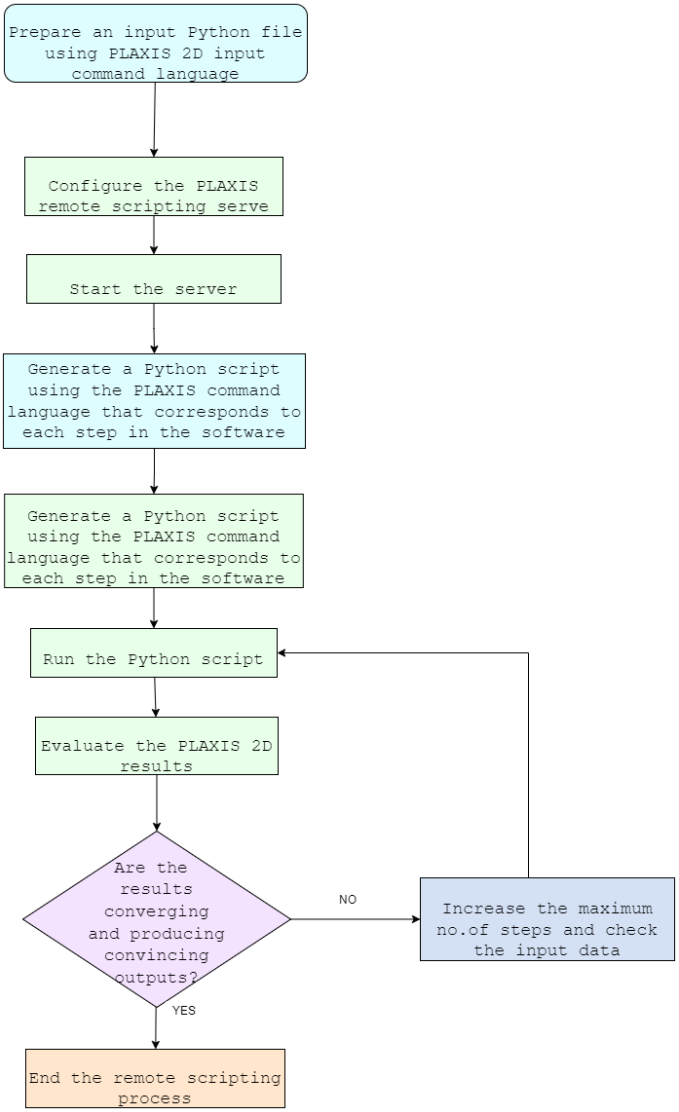

Figure 2.15: Flowchart depicting remote scripting

2.11 USDA soil texture classification

The United States Department of Agriculture (USDA) soil classification divides soil into three main categories: sand, clay, and silt, based on the size of particles passing through a 10 mm sieve (USDA, 2016). This classification system utilizes a triangular chart displaying twelve basic texture classes, including sand, sandy loam, loam, sandy clay loam, sandy clay, silt loam, silt, clay loam, silty clay loam, clay, and silty clay as shown in *figure 2.16*. Soil texture indirectly indicates the water retention capacities of the soil by emphasizing the distribution of grain sizes. Unlike changing properties such as soil moisture content, soil texture is considered a stable characteristic of soil that remains constant regardless of seasonal variations.

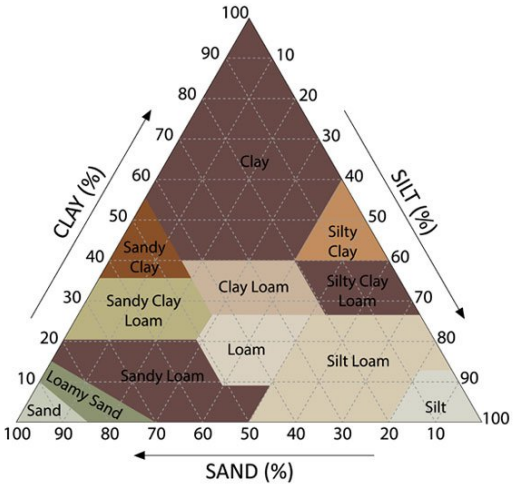

Figure 2.16: USDA-Triangular chart representing soil texture Classification (USDA, 2016)

2.12 Fully coupled flow-deformation analysis

In order to evaluate the development of pore water pressures and deformation concurrently in both saturated and unsaturated soil zones, a fully coupled flow-deformation analysis is often carried out (Bentley, 2020). These changes are caused by changing hydraulic boundary conditions over time. In fully coupled flow deformation analysis, the predominant focus is on total pore pressures, which are the sum of steady-state pore water pressures and excess pore pressures. This differs from consolidation analysis, which primarily impacts the excess pore pressures. At the end of the calculation stage, the steady-state pore water pressures are first determined based on the groundwater flow conditions in order to ensure consistency in the investigation. The excess pore pressures can be back-calculated from the total pore pressures by this procedure. In general, the suction in the unsaturated zone above phreatic level and the behaviour of partially saturated soil are taken into account in the fully coupled flow deformation analysis. This is the most comprehensive and

precise analysis that takes into account the unsaturated zone's decreased permeability and saturation level. Thus, it is crucial to un-check the "Ignore Suction" option when performing a fully coupled flow-deformation analysis to accurately measure matric suction. However, the "Ignore Suction" option can be utilised to regulate positive pore pressures in the unsaturated zone.

3

Derivation of Geotechnical parameters

This chapter focuses on deriving geotechnical parameters for an unsaturated silty slope, used in slope stability analysis. Some parameters were estimated based on typical values for silt and were considered sufficiently accurate for the study, as they do not influence flow calculations. Furthermore, the Van Genuchten parameters, which play a crucial role in influencing groundwater flow in the soil profile, were derived from the soil-water characteristic curve (SWCC).

3.1 Estimation of parameters

During geotechnical analysis, precisely interpreting the test results and extracting geotechnical input parameters from the test results is a crucial step. These parameters are then utilized in geotechnical numerical analyses, which involve defining appropriate boundary condition (Öberg, 1997). The geotechnical parameters describing the mechanical behavior of soil include bulk density, friction angle, moisture content, void ratio, Poisson's ratio, Young's modulus, and cohesion coefficient. The bulk density of saturated soil, along with the friction angle and moisture content, were obtained from the CPT results conducted at the Skedomsravinen test site. These results indicate that the typical bulk density of saturated soil is $1.9\,\mathrm{t/m^3}$. The water content of the soil is 15%, and the friction angle is 34°. The specific gravity values for various soils are provided in Appendix A. According to this data, the specific gravity of silt is evaluated to be 2.67 (Roy and Bhalla, 2017). Specific gravity of soil is defined as the ratio of the density of soil solids to the density of water. This fundamental, dimensionless property is crucial in soil mechanics and geotechnical engineering. Specific gravity plays a key role in determining various other soil properties, such as soil density, void ratio, and degree of saturation . The density of water is considered as $1000\,\mathrm{kg/m^3}$ and the density of soil is calculated using the equation 3.1 (Delwyn.G.Fredlund et al., 2012).

$$Specific\ gravity, G = \frac{\rho_{solid,soil}}{\rho_{water}} \tag{3.1}$$

While the saturated unit weight of silt is calculated from the bulk density, the dry unit weight of silt is taken from the laboratory test results of Skedomsravinen test site, whose value is $16\,\mathrm{kN/m^3}$. The index properties of the soil which includes void ratio and porosity are computed using the equation 3.2 and 3.3. The Poisson's ratio

and Young's modulus for silt soil are determined based on the typical value ranges provided in the Appendix A. For silt, a Poisson's ratio of 0.3 and a Young's modulus of 15 kPa are assumed (Budhu, 2010).

$$Void\ ratio, e = \frac{\rho_{solid,soil} * (1 + w)}{\rho_{bulk}} - 1 \tag{3.2}$$

$$Porosity, n = \frac{e}{1 + e} \tag{3.3}$$

Matric suction is a crucial parameter in unsaturated soil mechanics and essential for predicting and maintaining the stability of slopes (Rahardjo et al., 2019). Matric suction enhances the cohesion in unsaturated soils, thereby increasing their shear strength. This significant strength contribution is particularly relevant for soils above the groundwater table. During rainfall, infiltration into the slopes causes the groundwater levels to rise, which decreases the matric suction and, consequently, affects the strength and stability of the slopes. The correlation between matric suction and degree of saturation provides insights into the behavior of unsaturated soils, a relationship often termed the Soil-Water Characteristic Curve (SWCC). Therefore, the matrix suction and degree of saturation utilized in the investigation were derived from laboratory and field investigation findings conducted at the Skedomsravinen site as shown in table 3.1.

Table 3.1: Matrix suction and degree of saturation (Öberg, 1997)

Matrix suction kPa	Degree of Saturation
0	1
0.101	1.00
4.848	0.877
9.607	0.742
14.554	0.493
19.124	0.432
28.371	0.343
37.375	0.323
1000000	0

The values presented have been extracted from the water retention curves obtained for the silt soil, which are detailed in the Appendix A. The soil suction typically ranges between zero to 10^6 kPa. In a typical SWCC for silt, the air-entry value is the matric suction at which air begins to displace water in the largest soil pores (Delwyn.G.Fredlund et al., 2012). As the soil requires increasing suction to remove additional water, the remaining water is referred to as the residual water content. The volumetric water content reaches saturation when the soil suction is zero, The corresponding water content is refereed to as saturated water content S_{sat}. Conversely, the volumetric water content reaches residual water content S_{res} at high-soil suction values.

3.2 Determination of Van-Genuchten parameters

The SWCC is utilized to characterize the hydraulic parameters governing groundwater flow in unsaturated soil. Various models have been introduced to fit the Soil-Water Characteristic Curve (SWCC) to predict the behavior of unsaturated soil. Some of the prominent models include those by Brooks and Corey (1964), Van Genuchten (1980) and Fredlund and Xing (1994). Among these, the van Genuchten model has gained popularity in groundwater literature and is widely used due to its flexibility in accurately rendering results for both disturbed and undisturbed soil samples. This model is suitable for both fine-grained and coarse-grained soil types. Therefore, the VG model's empirical equation will be used to fit the SWCC. As, the numerical analysis of the slope is performed in PLAXIS, the preferred choice is to utilize the VG empirical equation embedded within the software. This is due to the discrepancy between the equation employed in PLAXIS and the general equation. PLAXIS has tailored the general VG equation with modifications to better align with the software's functionalities and user requirements. However, the fundamental principles governing the relationship between water content and soil suction, as defined by the VG equation, remain unchanged. In PLAXIS, the VG equation is a closed-form equation of three-parameters, that depicts the correlation between the degree of saturation and pressure head as shown in equation 3.4 (Bentley, 2015). The equation yields accurate results for low and intermediate suctions.

$$S(\phi_p) = S_{res} + (S_{sat} - S_{res})\left[1 + (g_a|\phi_p|)^{g_n}\right]^{g_c} \tag{3.4}$$

The g_a is associated with the air-entry value and influences the shape of the retention curve, g_n represents the pore size value and g_c corresponds to the asymmetry of the model and functions as a factor of residual saturation (Bentley, 2015). When the suction pore stress is divided by the unit weight of the pore fluid, it is referred to as the pressure head (ϕ_p). Since suction represents the negative pore pressure that holds the water in the soil pores, the pressure head reflects this by being negative sign as shown in equation 3.5.

$$\phi_p = -\frac{p_w}{\gamma_w} \tag{3.5}$$

In PLAXIS, the three-parameter VG equation has been simplified to a two-parameter equation by making the following assumptions as illustrated in equation 3.6 (Bentley, 2015).

$$g_c = -\frac{1 - g_n}{g_n} \tag{3.6}$$

Several approaches have been developed by researchers to analytically solve theoretical models for evaluating the hydraulic properties of unsaturated soil. Van Genuchten (1980) and Brooks and Corey (1964) have devised methods for determining parameters to estimate hydraulic functions. R.H.McCuen et al., 1981 conducted a statistical analysis using Brooks and Corey (1964) equations on USDA soil texture classifications, to evaluate the water holding capacity of different soil textures. They

provided mean and standard deviation values for each soil texture type regarding their soil-water retention characteristics. The USDA classification can serve as a parameter for estimating soil texture types, except for silt. The water holding capacity of silt can be extrapolated from values provided for other soil types. The USDA soil texture classification is provided in the chapter 2.11. Furthermore, an to this research was conducted to determine the influence of soil parameters on the Brooks-Corey parameters, apart from soil textures, revealing that soil composition played a significant role in parameter variation of the Brooks-Corey equation (1964). Using this as a basis, a similar approach has been developed with the Van Genuchten equation. The four-parameter VG equation is employed to evaluate the water retention capacity of different soil textures. The parameters for soil water retention characteristics are derived from soil properties monitored in soil survey reports, regression equations, and other sources. Carsel and S.Parrish, 1988 introduced a method for constructing probability density functions for various water retention characteristics across 12 soil texture groups. They provided values in a range for different Van Genuchten parameters to describe the hydraulic functions, as illustrated in a table 3.2. The parameters g_a and g_n in the Van Genuchten equation can vary depending on the soil type. The type of soil texture can be determined when the values of the VG parameters are known or vice-versa. However, it's important to note that these ranges serve as general guidelines, and specific values for a given soil may vary. Hence, it is necessary to calibrate these parameters based on experimental data for any particular soil.

Table 3.2: Ranges of g_a and g_n for Different Soil Types (Carsel and S.Parrish, 1988)

S.No	Soil Type	g_a (m^{-1})		g_n	
		Min	Max	Min	Max
1	Sand	1.4	14.5	1.56	2.68
2	Loamy sand	3.41	12.4	1.37	2.28
3	Sandy loam	3.6	7.5	1.23	1.89
4	Loam	1.0	3.6	1.25	1.56
5	Silt	0.4	1.6	1.29	1.37
6	Silty loam	0.4	2	1.29	1.41
7	Sandy Clay loam	0.7	5.9	1.17	1.48
8	Clayey loam	0.9	1.9	1.09	1.31
9	Silty Clayey loam	0.5	1	1.09	1.23
10	Sandy Clay	0.5	2.7	1.09	1.23
11	Silty clay	0.3	0.5	0.42	1.09
12	Clay	0.4	0.8	0.3	1.09

3.2.1 Establishing SWCC

The matrix suction and degree of saturation values determined from the water retention curves at the Skedomsravinen site were used to establish SWCC. The Van Genuchten (VG) equation, a widely adopted model for describing the SWCC and

hydraulic behaviour of unsaturated soil, was employed in PLAXIS software, with the representation shown in Equation 3.4. To calculate the pressure head, Equation 3.5 was utilized. A standard unit weight of weight, $10\,\mathrm{kN/m^3}$ was assumed for the analysis. At zero suction, the maximum saturation is considered to be 1, while at high suction values, the residual saturation is assumed to be zero. The parameter g_C, representing the asymmetry of the SWCC, was evaluated using Equation 3.6. Once all the input parameters are evaluated, a Python script has been created using the VG equation in PLAXIS to establish the SWCC. The program is coded to extrapolate the parameters g_a ,g_n and g_C from the curve. These VG parameters will then be used to simulate the groundwater behavior in the unsaturated silt slope during a fully coupled deformation analysis in PLAXIS under the influence of rainfall. By integrating the VG parameters derived from the SWCC, PLAXIS can more accurately predict the complex interactions between soil, water, and structural elements, providing valuable insights for geotechnical engineering designs and risk assessments in slope stability investigations. The SWCC explaining the relationship between the matrix suction and degree of saturation is shown in the *figure 3.1.*

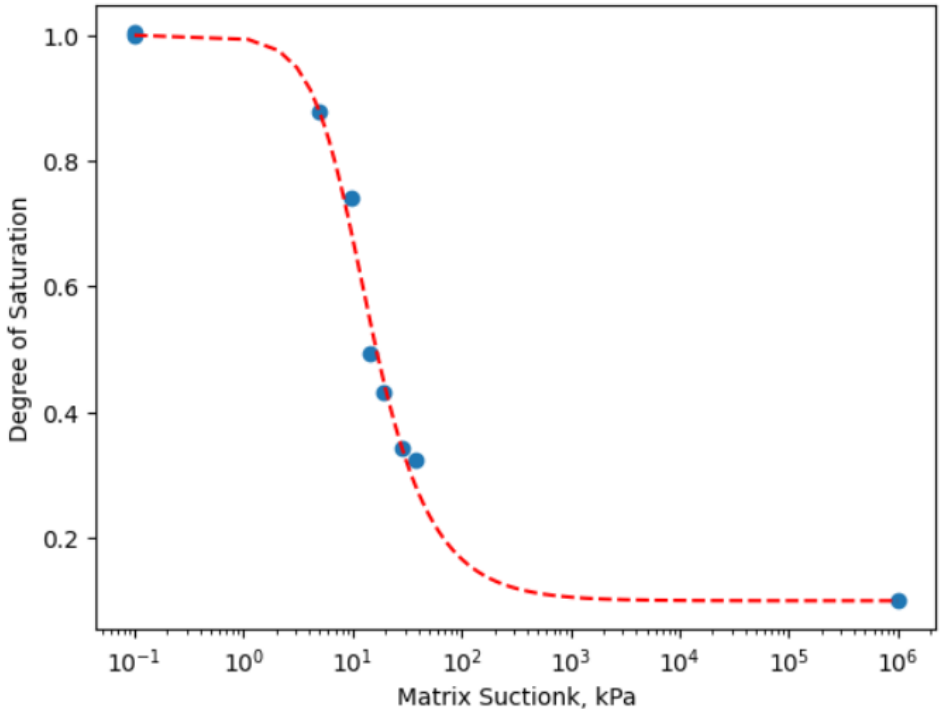

Figure 3.1: SWCC for silt

The VG parameters extracted from the curve are as follows: g_a =0.859, g_n = 2.060 and g_m = 0.515. Upon comparison with the value ranges specified for each soil texture in table 3.2, it is observed that these parameters fall within the range associated with silt.

3.3 Annual Precipitation data

The *figure 3.2* illustrates the annual precipitation measurements, highlighting seasonal variations throughout the year 1995. A precipitation level of 60mm is regarded as typical. The highest recorded precipitation, reaching 80mm, occurred in February 1995. Notably, there was no precipitation during the summer months of April, May, and June. The fully coupled deformation analysis of slope stability under the influence of rainfall will be conducted through advanced numerical simulations in PLAXIS 2D, incorporating the precise annual precipitation data for meticulous evaluation will be carried out in chapter 4. The precipitation data, converted to units compatible with PLAXIS software, is presented in Appendix A.

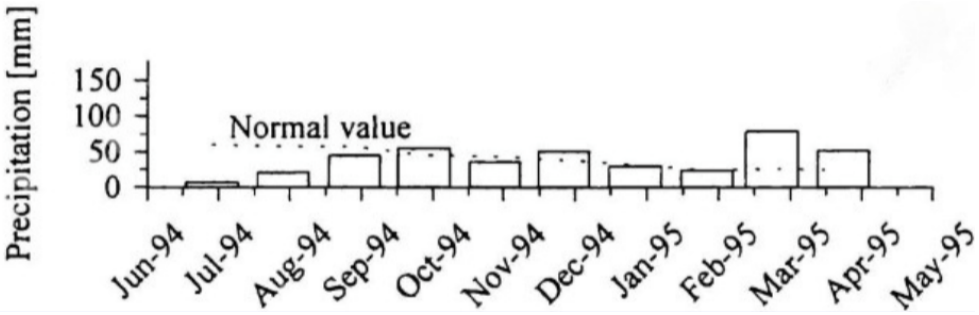

Figure 3.2: Annual precipitation measurements (Öberg, 1997)

3.4 Saturated permeability

The saturated permeability, also known as hydraulic conductivity, refers to the soil's capacity to allow water to flows through it (C.W.Fetter, 1988). This property is quantified by the coefficient of permeability, denoted as k. When water flow occurs parallel to the geological formation plane, it is termed horizontal permeability k_x. Conversely, when the flow is perpendicular to the geological formation plane, it is termed vertical permeability k_y. In this investigation, it is assumed that the horizontal and vertical permeability are equal, i.e., $k_x = k_y$. This assumption simplifies the analysis, allowing for uniform permeability characteristics throughout the soil conditions. The saturated permeability of silt is evaluated based on the grain-size distribution obtained from laboratory sieve analysis test results conducted at the Skedomsravinen test site using the Hazen's equation 3.7.

$$k = C(d_{10})^2 \tag{3.7}$$

4
Numerical Modelling

This section focuses on the numerical modeling of the unsaturated slope using PLAXIS 2D software and Python remote scripting to investigate the effect of rainfall on the stability of the unsaturated silt slope. Additionally, it presents the geometry of the soil profile and the geotechnical parameters used in the analysis. Furthermore, this section briefly discusses the numerical analysis of the unsaturated slope carried out in PLAXIS 2D, along with the sensitivity analysis performed on the strength parameters, Van Genuchten (VG) parameters, and the geometry of the slope.

4.1 Geometry of the slope

The unsaturated silty slope is modelled and analyzed in PLAXIS 2D version V22.01 using Python remote scripting. The initial rectangular soil contour is established to match the slope profile, and the geometry of the unsaturated slope is illustrated in the *figure 4.1*. The slope is modeled under 2D plane strain conditions. For numerical simulation, the slope elements are discretized using 15-noded triangular elements. The slope has a height of 54 meters and an inclination angle of 32°. The geotechnical parameters of the mechanical and groundwater flow parameters assigned to the soil profile are presented in the table 4.1.

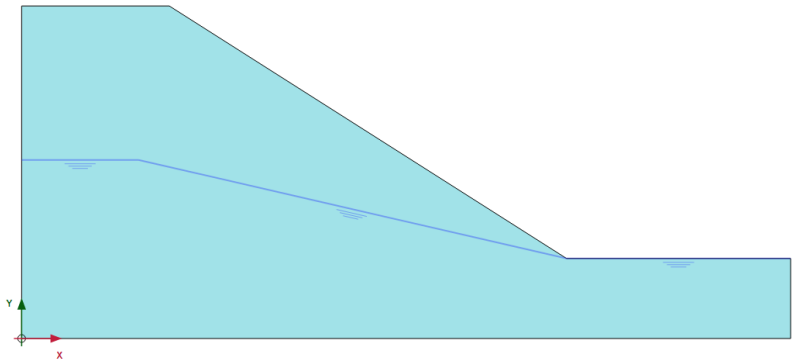

Figure 4.1: Geometry of the slope modelled in PLAXIS 2D

The hydraulic behavior of the soil is characterized in the model through the selection of a user-defined classification type and the utilization of the Van Genuchten method for fitting the SWCC. The Van Genuchten parameters derived from the SWCC, as detailed in section 3.2.1, are used in the numerical analysis to replicate the hydraulic behavior. The hydraulic properties of the soil and the VG parameters are presented

in table 4.2. These soil properties are developed in the soil mode within the PLAXIS software. The phreatic level is located 25 meters below the ground surface and gradually decreases to 41 meters from the ground surface, which is defined in the flow conditions tab in the software. Once the model geometry is fully defined, it is divided into numerous finite elements for finite element analysis. A very fine element mesh of element size 0.03 is selected from the predefined element distribution, resulting in the generation of 701 elements and 5811 nodes as shown in *figure 4.2*. The generation of the mesh relies entirely on a robust triangulation procedure.

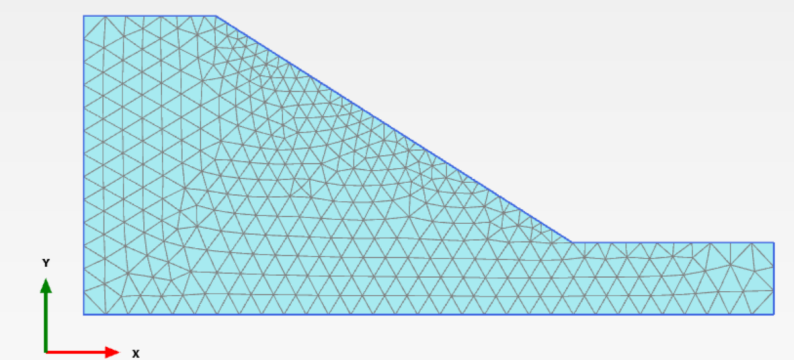

Figure 4.2: Mesh configuration in PLAXIS 2D

In PLAXIS, a drained analysis of the unsaturated slope is performed by selecting the predefined options to specify the drained behavior of silt. In drained material behavior, the stiffness and strength properties of the soil are defined using effective values. Furthermore, the soil behavior is approximated by choosing the Mohr-Coulomb failure criterion to reflect perfectly elastic properties. Additionally, default settings have been employed for the thermal and initial properties of the soil. The cross permeability is configured as impermeable to restrict cross-flow of water.

Table 4.1: Mechanical properties of soil

Soil Parameters	Values	Unit
Material Definition	Silt	-
Drainage type	Drained	-
Soil Model	Mohr-Coulomb	-
γ_{unsat}	16	kN/m^3
γ_{sat}	19	kN/m^3
e_{init}	0.64	-
n_{init}	0.39	-
E'_{ref}	15000	kN/m^2
c'_{ref}	3	kN/m^2
ϕ'	34°	-
ν	0.35	-
ψ	0	-

Table 4.2: Groundwater flow properties of soil

Soil Parameters	Values	Unit
Model Classification	User-Defined	-
Model Type	Van-Genuchten	-
S_{sat}	1	-
S_{res}	0	-
g_n	2.06	-
g_a	0.859	1/m
g_l	0	-
k_x	0.7266	m/day
k_y	0.7266	m/day
ν	0.35	-

4.2 Boundary Conditions

The model is equipped with flow boundary conditions and mechanical boundary conditions tailored for conducting a fully coupled flow-deformation analysis, as detailed in the table 4.3. In fully coupled deformation analysis, flow boundary conditions typically denote areas where pore water can ingress into or egress out of the soil (Bentley, 2020). Groundwater flow is restricted at the bottom layer of the slope by designating it as an impervious layer with a closed boundary. Conversely, groundwater flow is permitted at the two vertical sides of the slope with an open boundary, indicating free-flow conditions. Moreover, the boundary at the top layer of the slope remains open to facilitate rainfall infiltration or seepage into the intermediate zone at subsequent depths below the ground surface. The mechanical boundary conditions impose a set of constraints that allows or restrict the deformation of the model in x and y direction (Bentley, 2020). The mechanical boundary conditions along the x-direction, $x_{\min}$ and $x_{\max}$, of the model are restrained from horizontal movement by assigning them a normally fixed boundary constraint, while allowing free deformation in the y-direction. The bottom layer of the model is restrained from deformation in all directions by assigning $y_{\min}$ as fully fixed. The top layer of the model is set free in all directions by assigning $y_{\max}$ as free.

Table 4.3: Flow boundary and mechanical boundary conditions

Boundary Direction	Mechanical Boundary Constrains	Flow Boundary constrains
$x_{\min}$	Normally fixed	Open
$x_{\max}$	Normally fixed	Open
$y_{\min}$	Fully fixed	Closed
$y_{\max}$	Free	Open

When performing a fully coupled deformation analysis, it is crucial to assign appropriate groundwater flow boundary conditions to the model. The bottom layer is set to a closed boundary, chosen from predefined options, which indicates that groundwater flow is restricted along this boundary. The two vertical boundaries are

assigned to seepage behavior, allowing groundwater flow along these boundaries. Since the analysis includes the effects of precipitation, it is important to set the flow boundary behavior of the top layer of the model (Bentley, 2020). When flow boundary conditions are specified for the top layer, they override the precipitation settings defined in the model conditions. This means that any precipitation details assigned in the model conditions will be ignored, as the flow boundary conditions always take precedence over model conditions.In this investigation, precipitation data are applied to the model by assigning vertical recharge to the ground surface under model conditions.

4.3 Vertical Recharge

The primary focus of the investigation is to examine the stability of the unsaturated silt slope under the influence of rainfall. In the fully coupled flow-deformation analysis conducted in PLAXIS 2D, the precipitation data described in Section 3.3 is utilized. This precipitation data is incorporated into the model as vertical recharge or infiltration at the top layer. The stability of the slope is studied using a constant discharge function rather than a time-dependent function. A rainfall intensity of 0.0027 m/day, which corresponds to the maximum precipitation recorded in February 1995, is applied to the model continuously over a period of 30 days to study the slope's stability. It's essential to note that the applied vertical recharge should be in positive values to encourage infiltration rather than evaporation. The maximum pore pressure head is set to -30m. Moreover, it's important to highlight that the vertical discharge applied to the ground surface is lower than the permeability of the soil. This observation is significant because when the applied precipitation is more than the soil permeability, it can result in water ponding on the slope surface, potentially leading to surface runoff of excess rainwater.

4.4 Numerical Analysis in PLAXIS 2D

The numerical analysis of an unsaturated soil slope, with geometry and parameters derived from relevant data, will be conducted to evaluate the stability of the slope under the effect of rainfall. Additionally, the investigation will focus on the effect of the SWCC on the stability of the unsaturated slope when subjected to rainfall. This numerical analysis will be carried out using PLAXIS 2D software, with the process automated through Python scripts created according to the PLAXIS Remote Scripting guidelines. The python codes used to perform the numerical analysis is illustrated in Appendix B under section B.1. Every step in the analysis will be automated through Python scripts designed to connect to PLAXIS via its API. The Python scripts will automate every step of the analysis, including:

- Creating a soil rectangular contour.
- Creating soil polygon.
- Creating and assigning material properties.
- Generating global groundwater level

- Defining and assigning flow boundary conditions and mechanical boundary conditions.
- Generating the mesh.
- Setting up calculation phases.
- Assigning precipitation data.
- Running the analysis to determine the factor of safety of the slope under initial conditions and under the effect of rainfall.

4.4.1 Calculation phases

The effect of SWCC on unsaturated slope stability under the influence of rainfall is evaluated in PLAXIS 2D software through numerical simulation conducted in four stages: Phase 0, Phase 1, Phase 2, and Phase 3. The calculation type, loading type , pore pressure type, maximum iteration steps used in calculating each phase is presented in a table 4.4

Phase 0 (Initial Phase): In the initial phase of stage construction, gravity loading is selected as the loading type. This choice is made because the stability analysis of the unsaturated slope involves a non-horizontal ground surface. Therefore, gravity loading is preferred over the K0 procedure for this investigation. Gravity loading is a type of plastic analysis in which the self weigh of the soil is used to establish the the initial stress conditions. This analysis involves calculating the steady-state water pressure using the phreatic surface, with inputs based on the global water level set in flow conditions. Furthermore, the "ignore suction" option is unchecked in this phase, as this approach accounts for the suction in the unsaturated zone above the phreatic level.The calculation for this phase uses the default setting of a maximum of 1000 steps. The soil polygon is activated in this step.

Phase 1 (Safety analysis): The next phase in the construction stage involves a safety analysis of the slope using the ϕ-c reduction approach. This phase follows Phase 0 and calculates the slope's factor of safety based on the initial stress conditions, considering the suction in the unsaturated zone, but not accounting for the effects of rainfall. The calculation uses the default step parameters, with a maximum of 100 steps. Since the initial stress conditions were based on gravity loading, the displacements in Phase 1 are reset to zero to prevent the initial stress effects from carrying over to subsequent calculation phases.

Phase 2 (Fully coupled flow-deformation analysis): This phase follows the initial Phase 0. It involves a fully coupled flow-deformation analysis, resulting in estimations for both deformation and groundwater flow. Precipitation data is activated in this phase, with the slope being analyzed for rainfall intensity over a period of 30 days. To achieve greater convergence, manual steps are assigned instead of using the default ones. The minimum iteration steps are set to 15 and the maximum iteration steps to 30 for the number of iteration involving 10,000 steps are utilised.

Phase 3 (Safety analysis after rainfall): This phase follows Phase 2, and it

involves analyzing the stability of the slope under the influence of rainfall. The factor of safety is calculated at the end of 30 days of constant infiltration of rainfall, and the results are compared with the factor of safety of the slope under the initial stress conditions. The calculation uses default iteration steps.

Table 4.4: Details of each staged construction phase of the analysis

Phase	Calculation Type	Loading Type	Pore pressure	Time interval
Initial Phase	Gravity Loading	Staged construction	Phreatic	-
Phase 1	Safety Analysis	Incremental multipliers	-	-
Phase 2	Fully Coupled Flow deformation	Staged Construction	-	30 days
Phase 3	Safety Analysis	Incremental multipliers	-	-

4.4.2 Slope Stability for derived VG parameters

The stability of the unsaturated slope will be investigated using the Van Genuchten (VG) parameters derived from the SWCC. The SWCC, which shows the relationship between matric suction and degree of saturation, will be plotted in Python using packages such as NumPy, Pandas, SciPy, curve_fit, and Pyplot.The slope will be analyzed for both initial stress conditions under gravity loading (Phase 1) and under the effect of infiltration (Phase 3) in association with the rainfall intensity mentioned in section 4.3. The Factor of Safety (FOS) of the slope will be obtained by conducting a safety analysis using the reduction method. If the slope tends to fail under the initial stress conditions in Phase 1, it is recommended to revise the parameters used in the analysis.

4.4.3 Stability analysis by iterating VG parameters

The stability of the unsaturated slope is analyzed for different Van Genuchten (VG) parameters to investigate the influence of the SWCC on the slope's stability in PLAXIS 2D using Python codes. The analysis is conducted using five different g_a and g_n values. The maximum and minimum values of g_a and g_n for various soil types, as specified in the Plaxis 2D reference model, are utilized for the analysis. The mean of the maximum and minimum values is calculated to obtain a baseline value. Additionally, the mean of of this baseline value, in combination with the minimum and maximum values, is utilized to determine the intermediate mean, resulting in five distinct sets g_a and g_n values for the analysis. The obtained g_a and g_n values are iterated to form a total of 25 combinations, as illustrated in the table 4.5, for use in the numerical analysis. The highlighted values denote the maximum and minimum g_a and g_n. These VG parameters are employed in conjunction with the soil properties detailed in the section 4.1. The unsaturated slope is analyzed solely under initial stress conditions and gravity loading using these parameters, while the impact of precipitation is disregarded for now but will be taken into account in subsequent analyses.

Table 4.5: Iterated VG parameter combinations

Iteration	g_a	g_n
Iteration 1	0.5	1.09
	0.5	1.48
	0.5	1.89
	0.5	2.28
	0.5	2.68
Iteration 2	3.6	1.09
	3.6	1.48
	3.6	1.89
	3.6	2.28
	3.6	2.68
Iteration 3	7.5	1.09
	7.5	1.48
	7.5	1.89
	7.5	2.28
	7.5	2.68
Iteration 4	12.4	1.09
	12.4	1.48
	12.4	1.89
	12.4	2.28
	12.4	2.68
Iteration 4	14.5	1.09
	14.5	1.48
	14.5	1.89
	14.5	2.28
	14.5	2.68

4.4.4 Stability Analysis: Infiltration

The stability of the unsaturated slope is significantly influenced by rainfall infiltration, which generally increases pore water pressure above the groundwater level, raises the unit weight of the soil, and decreases matric suction and shear strength (Delwyn.G.Fredlund et al., 2012). These changes may have a significant impact on the slope's FOS, which might result in slope failures. The distribution of moisture content and matric suction due to rainfall is crucial for unsaturated slope stability. So, employing different iterated VG parameters together with the same soil properties, slope geometry and flux boundary conditions as specified in the section 4.1 and 4.2, the stability of the unsaturated slope under the influence of rainfall will be examined in PLAXIS 2D using python remote scripting. The influence of g_a and g_n on the stability of an unsaturated slope under rainfall will be investigated using fully coupled flow deformation analysis and safety analysis. The investigation will be conducted over a period of 10 days with a constant rainfall intensity of 0.0027 m/day and a maximum pore pressure head of -30. To observe the influence of VG parameters on slope stability, FOS will be recorded each day throughout the 10-day

period. The stability of the slope will be iterated for various combinations of g_a and g_n values, as referred in the table 4.5.

4.5 Sensitivity analysis

The sensitivity analysis of the unsaturated slope is carried out in PLAXIS 2D using Python remote scripting to evaluate how varying the slope angle and shear strength of the soil simultaneously affects the stability of the unsaturated slope under rainfall conditions. The sensitivity of the slope's geometry and shear strength when subjected to various VG parameters will be investigated for all possible combinations of VG parameters. Using the original slope's soil parameters, the slope is analysed under drained circumstances in all cases. During a 10-day period of steady rainfall, the geometry and shear strength angle of the slope will be changed in order to examine variations in the FOS. The influence on the FOS will be studied for every single day over the entire 10-day period for each set of VG parameter combinations.

4.5.1 Geometry Sensitivity

The geometry of the slope, groundwater conditions, and mechanical and shear strength properties of the soil are usually taken for consideration in slope stability analyses, which highlight the significance of the slope angle for evaluating stability. Usually, altering the slope angle results in a change in the height of the slope, producing a modified geometry. In this investigation, three different slope angles will be used to modify the height of the slope, and the changed geometries will be numerically analyzed in PLAXIS 2D. The original slope has a slope angle of 32° and a total height of 54 meters. This investigation will decrease the slope angle from its original value to observe the effects on slope stability. The three different slope angles and the corresponding slope heights are illustrated in the table 4.6 and the geometric dimensions of the slope is depicted in *figure 4.3* . Further, the geometry of the slope for varied slope angle is illustrated in *figure 4.4*, *figure 4.5* and *figure 4.6*.

Table 4.6: Iterating Slope angle and slope height

Slope angle(α)	Width of slope (m)	Height of slope(m)	Total height of slope(m)
20°	64.5	23.5	36.5
25°	64.5	30.07	43.1
30°	64.5	37.23	50.2

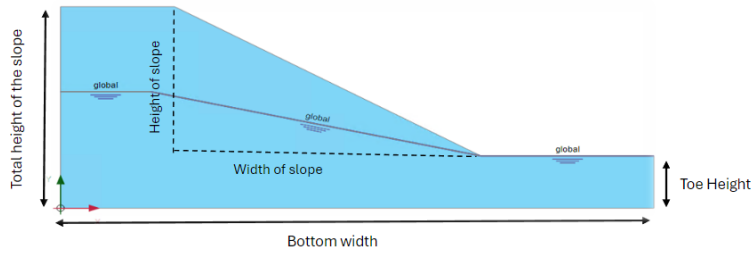

Figure 4.3: Geometric dimensions of the slope

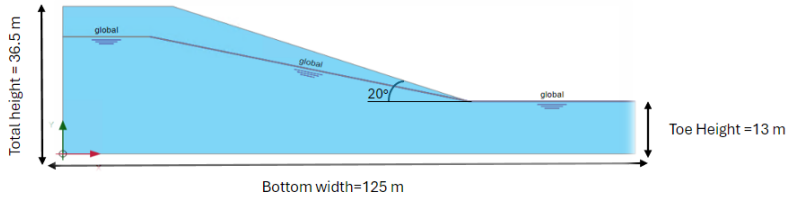

Figure 4.4: Geometry of the slope: α =20°

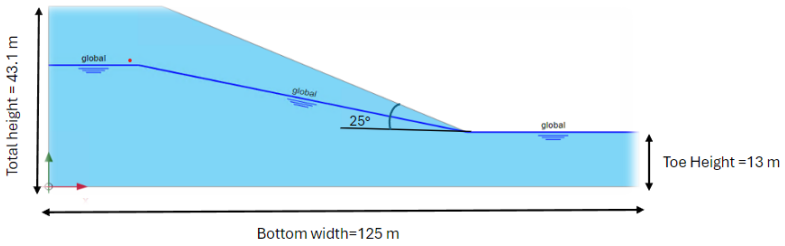

Figure 4.5: Geometry of the slope: α =25°

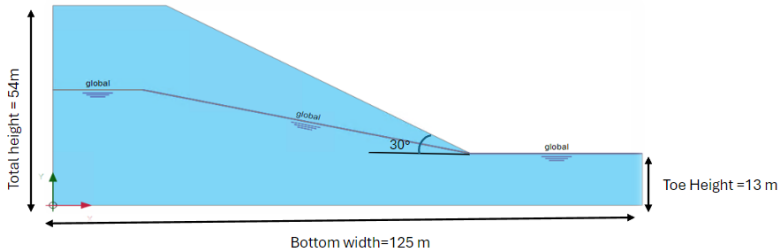

Figure 4.6: Geometry of the slope: α=30°

4.5.2 Shear strength sensitivity

To investigate the effect of shear strength parameters on the stability of unsaturated soil, three different shear strength parameters, precisely the friction angle ϕ, such as 25°, 30° and 35° will be considered. The stability of the unsaturated slope will be evaluated for these three friction angles (ϕ) under rainfall conditions, while retaining the remaining original soil properties and flux boundary conditions. The effect of the friction angle on the slope's stability will be studied in conjunction with varying slope geometry whose values are mentioned in the table 4.6. This analysis will be conducted for each of the 25 combinations of VG parameters, considering the infiltration of steady rainfall over a period of 10 days.

5

Results and Discussions

This chapter presents the findings of the numerical analysis of the unsaturated slope during rainfall infiltration under the influence of the SWCC using PLAXIS 2D remote scripting. Additionally, the findings of the sensitivity analysis will be examined, focusing on how changes brought to soil's geometry and shear strength parameters affect the stability of the unsaturated slope. A graph displaying the safety factor that was determined through numerical analysis will be provided for discussion.

5.1 Unsaturated Slope Stability Validation using PLAXIS 2D

The results of the failure surface of the slope under gravity loading is presented in the *figure 5.1*. The total displacements in the soil, reaching a maximum value of 9 meters, reflect the slip surface of the slope under initial stress conditions. The circular shape of the slip surface contributes to the homogeneity of the soil.

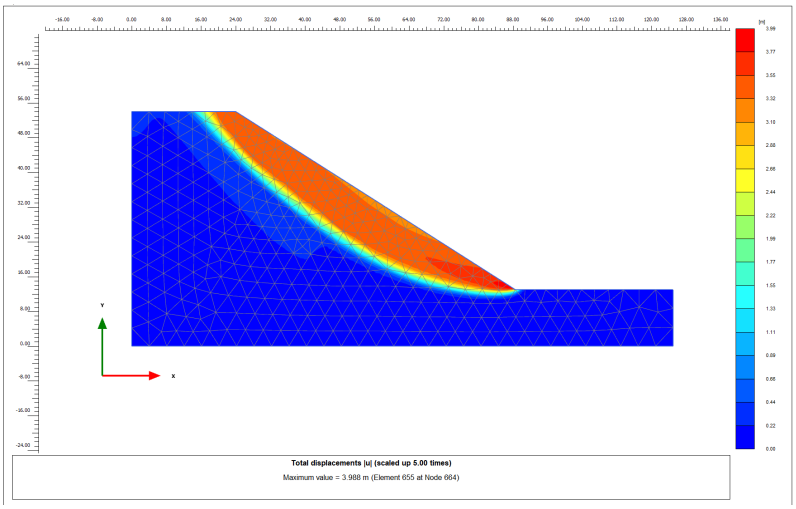

Figure 5.1: Total displacement of the Slope section under gravity loading (Phase 1)

The slip surface of the slope under the effect of rainfall infiltration for a period of 30 days is depicted in the *figure 5.2*. The slip surface appears circular in shape, and

it is visualized by means of total displacements of value 1.728 m resulting from the rainfall.

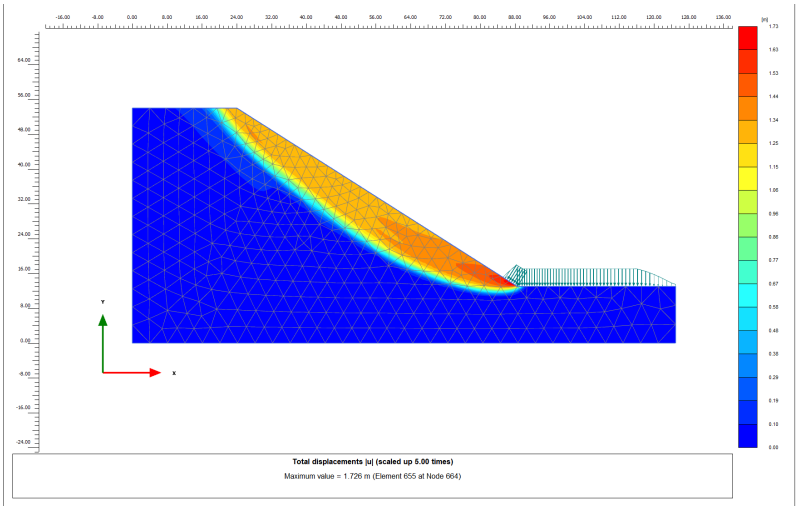

Figure 5.2: Total displacement of the Slope section under rainfall (Phase 3)

The present investigation used the phi-c reduction approach in PLAXIS safety analysis to determine the FOS of the slope. The FOS is plotted against the step size, with separate graphs for each calculation phase. The FOS of the unsaturated slope under gravity loading is initially 1.19. It is observed that the FOS drops to 1.12 at step size 40 and maintains this constant value until step 60 as shown in *figure 5.3*. This represents a 5.88% drop in FOS from the initial value, which can be attributed to initial stress redistribution in the slope under initial stress conditions analyzed under gravity loading. The FOS > 1 indicates that the slope remains stable under initial conditions. This suggests that the stability of the unsaturated slope for the employed soil parameters is sufficient for initial stress conditions.

The FOS of the slope under the effect of rainfall for a time-interval of 30 days is initially found to be 1.108 and drops to 1.05 as the step size increases as shown in *figure 5.4* . The drop in FOS can be attributed to the decrease in negative pore water pressure brought on by increased rainwater infiltration. This decrease impacts the soil's shear strength and, in turn, the slope's stability. In addition, the fact that the FOS is marginally larger than 1 implies that the slope is relatively stable. However, these findings can vary based on the type of infiltration pattern (i.e., time-dependent) or the intensity and duration of the rainfall.

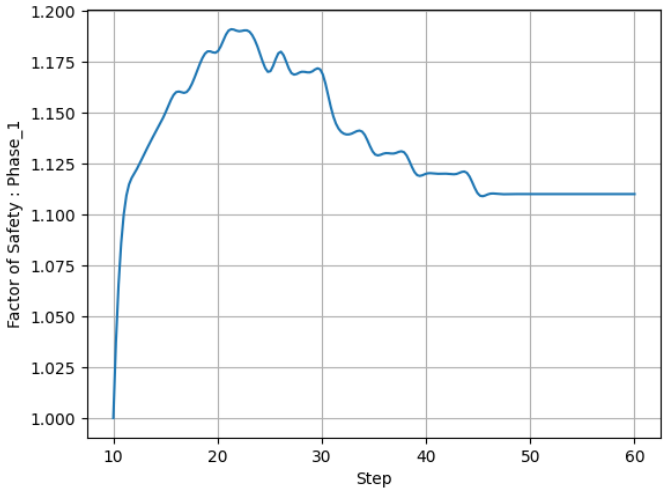

Figure 5.3: Stability of the slope under gravity loading

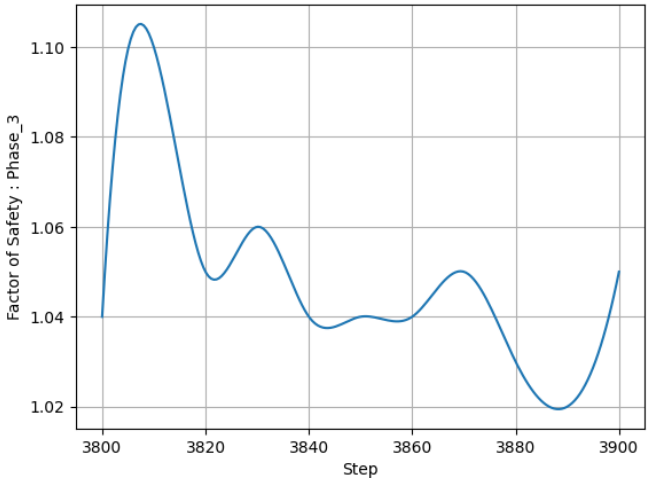

Figure 5.4: Stability of the slope under rainfall

The variation of suction along the slope under initial stress conditions is illustrated in the *figure 5.5*. It is notable that high suction, reaching 262 kN/m^2, is observed at the crest of the slope under the initial stress conditions, while very low to zero suction is detected below the groundwater table. The considerable disparity in suction levels across the unsaturated zone, particularly with elevated suction levels at the crest compared to the middle and toe of the slope, can be attributed to the fluctuation of moisture content along increasing depths of the slope. Above the groundwater table, the matrix suction remains relatively low, ranging between 40 kN/m^2 - 60 kN/m^2. This is likely due to the rise of water through capillary action, filling the pores in the capillary zone. As one moves towards the ground surface, the suction gradually increases due to lower degrees of saturation and the presence of more air-filled voids. Further, these high suction values effectively enhance the load-carrying capacity of the soil, consequently resulting in a notable increase in the Factor of Safety (FOS) of the slope.

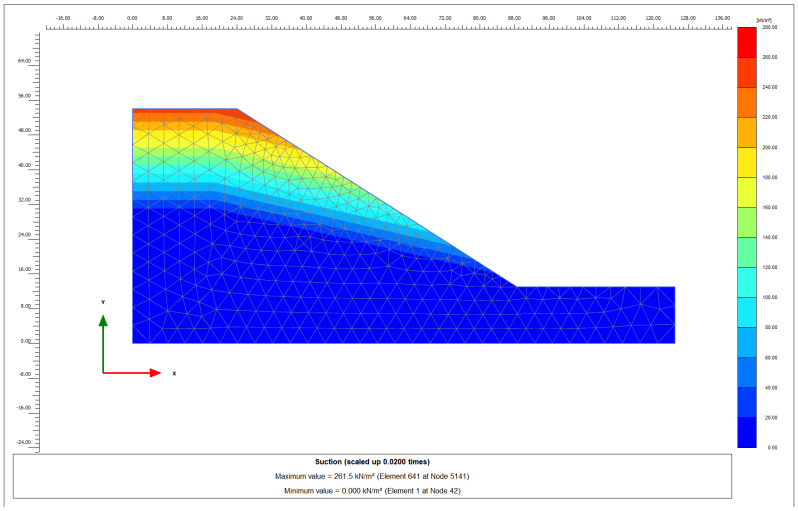

Figure 5.5: Suction profile for unsaturated slope under gravity loading

The suction value drops from 262 kN/m^2 to 0 kN/m^2 - 60 kN/m^2 at the crest of the slope when subjected to rainfall infiltration as shown in *figure 5.6* . Prior to rainfall, the crest of the slope exhibited high suction values, but a sudden drop in suction is observed at the onset of rainfall. The change in suction values is more significant at few meters below the ground surface and as approaching the initial conditions. Suction values of 204 kN/m^2 are found a few meters below the ground surface, indicating a 22.14% drop from the initial values. Furthermore, because of the extended period of rainfall, the change in suction is more noticeable at lower depths. However, there is no apparent variation in suction is observed at the middle and toe of the slope.

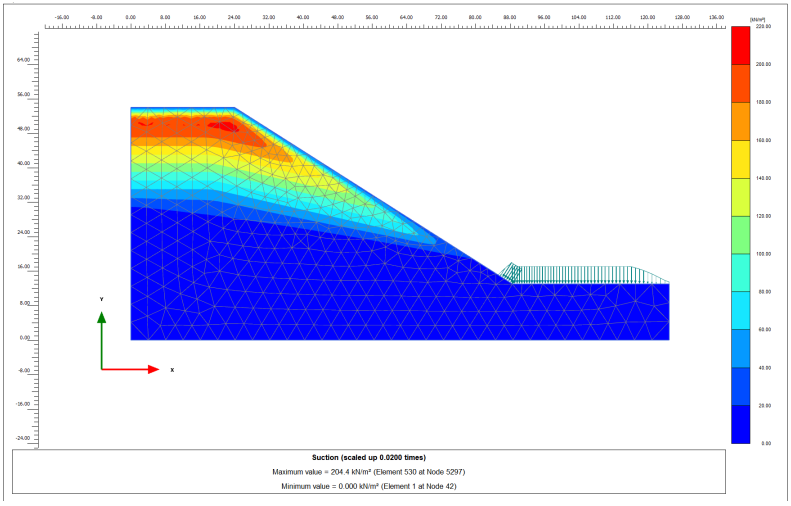

Figure 5.6: Suction profile for unsaturated slope under rainfall

5.2 Results for derived VG parameters

The stability of the unsaturated slope was investigated for 25 combinations of VG parameters under initial stress conditions. The effect of rainfall infiltration was completely disregarded, and the FOS for each distinct set of g_a and g_n values was determined through safety analysis, considering only the self-weight of the soil. The obtained FOS for each set of VG parameters is plotted in a 3D graph using the Python package Plotly, as shown in the figure.

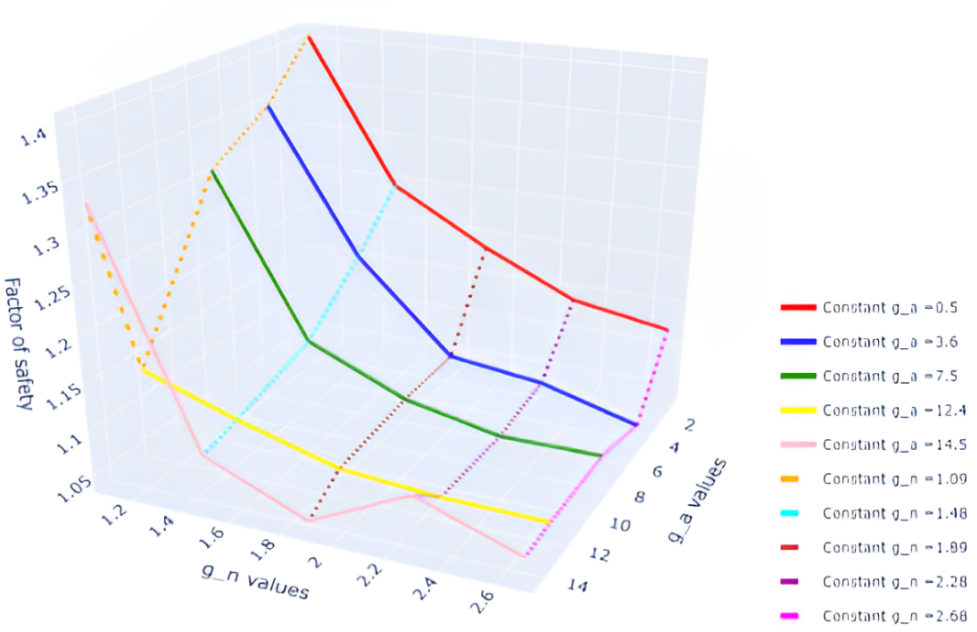

Figure 5.7: Effect of VG parameters on slope stability under initial stress conditions

In the graph, the solid lines represent the FOS values recorded by keeping the g_a values constant while varying the $g_n$values. The dotted lines represent the FOS values when g_n values are kept constant and g_a values are iterated. The maximum FOS of 1.403 is observed for $g_a = 0.5$ and $g_n = 1.09$ which are the minimum values in their respective ranges. Conversely, the slope shows a minimum FOS of 1.043 when $g_a = 3.6$ and $g_n = 2.68$. Additionally, the 3D graph indicates that when either of the VG parameter is kept constant and the other parameter is increased from its minimum to maximum value, the FOS of the slope decreases. For example, when g_a is held constant at any value within the range of 0.5 to 14.5 and g_n is varied across five different values from 1.09 to 2.68, the FOS demonstrates a gradual decrease. This trend is depicted by the solid lines in the graph. However, this prediction is not applicable in two specific cases: when $g_a = 14.5$ is kept constant and g_n is iterated to 2.28, and when $g_n = 1.09$ is kept constant and g_a is iterated to 14.5. In these scenarios, the FOS shows a sudden spike in values, indicating an anomaly when these parameters are used as inputs. Furthermore, it is observed that when g_a is kept constant at each value in the range from 0.5 to 14.5 and iterated for different g_n

values, the FOS is high when the constant g_a value is at its minimum. Conversely, when g_a is high, the FOS is low. This pattern also applies when g_n is kept constant and g_a is varied. Thus, the final conclusion is that both g_a and g_n values are inversely proportional to the FOS of the slope under gravity loading. This prediction is only valid when the slope is tested under initial stress condition.

5.3 Validation of stability results for derived VG parameters under rainfall

To explore the stability of an unsaturated silt slope under varying Van Genuchten (VG) parameters amidst rainfall influence, the slope undergoes analysis for 25, VG parameter combinations during steady rainfall infiltration over 10 days using PLAXIS 2D Python remote scripting. This study also delves into the impact of modifying one of the Van Genuchten (VG) parameters—either g_a or g_n, while keeping the other constant during a ten-day rainfall period. The purpose is to determine which parameter most significantly affects the FOS under rainfall conditions and to gain a comprehensive understanding of how these changes influence slope stability. g_n. The initial VG parameters derived from the SWCC are g_a =0.859 and g_n = 2.060. Subsequently, five different values for each parameter are generated by incrementally increasing and decreasing from the original values. The slope undergoes safety analysis using these varied VG parameter sets in PLAXIS 2D.

The *figure 5.8* presents a 2D graph plotted using Python packages such as matplotlib and pyplot. It illustrates the effect on the FOS of the unsaturated slope under varying g_n values within a specified range for each g_a value from 0.5 to 14.5 during the rainfall period. The 2D plot displays the variation of FOS against the length of the rainfall in days. Analysis of the 2D plots reveals the significant influence of the Van Genuchten parameter g_n on the FOS of the unsaturated silt slope under rainfall flux boundary conditions.Across all five graphs, a consistent trend emerges: as the g_n value increases, there is a notable decrease in the Factor of Safety (FOS). Additionally, for each g_n value, the FOS is high at the onset of rainfall activity and gradually reduces from day 1 to day 10. This decrease is particularly pronounced during the initial 1-5 days of rainfall, after which the rate of decrease slows down. Moreover, slopes with larger g_n values exhibit a slower rate of decrease in FOS compared to those with smaller g_n values. For instance, in *figure 5.8* (b), for the lowest g_n , the slope maintains relatively high FOS 1.3 at the early stage of rainfall and gradually decreases to a FOS of 1.172 after 10 days of infiltration. However with highest g_n values, the FOS starts declining after the 6th day of rainfall, eventually leading to slope failure. This occurs because the parameter g_n signifies the pore-size distribution of the soil. Moreover, when g_n is set to 1.09 for constant g_a values of 7.5 and 14.5, the soil mass collapses, resulting in the absence of a recorded factor of safety.

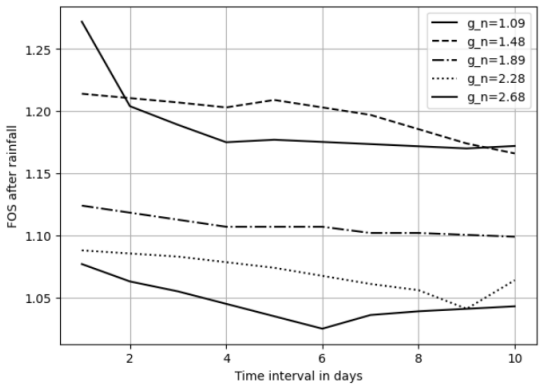

(a) $g_a = 0.5$

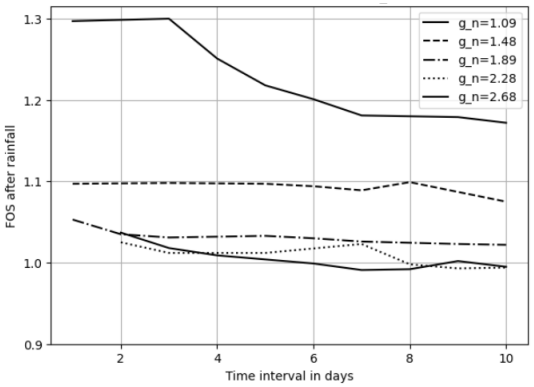

(b) $g_a = 3.6$

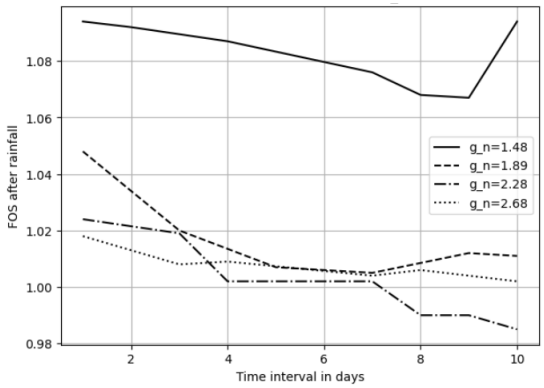

(c) $g_a = 7.5$

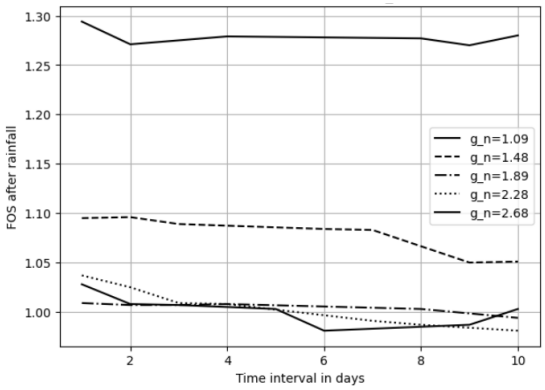

(d) $g_a = 12.4$

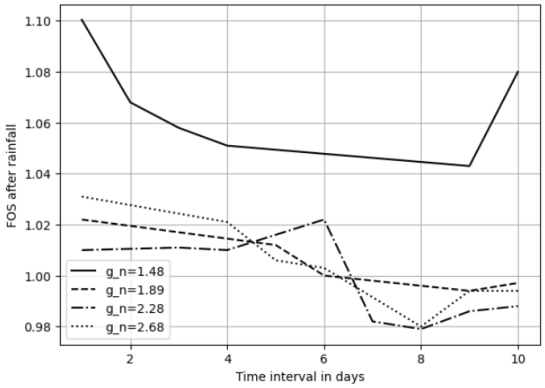

(e) $g_a = 14.5$

Figure 5.8: Effect of g_n values on the FOS of the slope measured for 10 days of time-interval

The *figure 5.9* illustrates the influence of g_a parameters on the FOS of an unsaturated slope subjected to a 10-day rainfall period. The g_a value represents the air-entry value (AEV) in the SWCC, indicating the point at which air begins to enter the soil pores in the unsaturated zone. This value is dependent on the type of soil considered. The graph clearly shows that g_a significantly impacts the FOS of the unsaturated slope. At low g_a values, the FOS is higher compared to high g_a values, where the FOS is lower. This phenomenon occurs because, at low g_a values, the soil particles in the slope are smaller. Consequently, when the slope experiences rainfall, the decrease in shear strength of of the soil is less pronounced for low g_a values. In contrast, at higher g_a values, the decrease in shear strength is much greater, resulting in a more substantial reduction in FOS. Further, at the onset of rainfall, the FOS gradually decreases with increasing g_a values. When accompanied by higher g_n values, such as 1.89, 2.28, and 2.68, the increase in g_a can lead to slope instability and failure. Additionally, the graphs marks a trend, where the FOS decreases linearly with increasing g_a values during the early stages of rainfall infiltration. However, as the infiltration period progresses and completes 10 days, the FOS shows a slight increase with higher g_a values. This indicates that the FOS initially decreases with increasing g_a values at the onset of rainfall, but shows a slight improvement in stability as the rainfall infiltration continues over time. Furthermore, it can be observed that for the lowest g_n value of 1.09, the soil tends to completely collapse when the g_a values are 7.5 and 14.5, resulting in the absence of FOS values for these combinations of VG parameters.

In a recent investigation by Fan and Zeng, 2016, a nuanced trend in the FOS values of unsaturated slopes when plotted against the duration of rainfall in hours was observed. The study delved into the influence of VG parameters on the stability of unsaturated slopes subjected to rainfall, employing a coupled hydro-mechanical analysis conducted in PLAXIS 2D. The research examined three distinct g_a values: 0.5, 2, and 7 (1/m), alongside three different g_n values: 1.1, 1.41, and 2. Each parameter's individual effect on slope stability during a 24-hour rainfall event was scrutinized. The findings highlighted the significant influence of both g_a and g_n values on the stability of unsaturated slopes. The findings suggest that while different g_a values exhibit no significant change in FOS values during the initial 10 hours of rainfall but a notable decrease in FOS is observed with prolonged infiltration upto 12 hours, particularly with lowerg_a values. Conversely, upon varying g_n values, they exhibit a significant impact on slope stability, with increasing g_a values the FOS decreases. The observed disparity between these previous results and those of present investigations may stem from the methodological approach. Past studies conducted by Fan and Zeng, 2016 focused on individual parameter assessments, whereas the present investigation considered the combined influence of two parameters. This disparity emphasises how crucial it is to take into consideration practical scenarios where several parameters interact simultaneously rather than simply one parameter at a time.

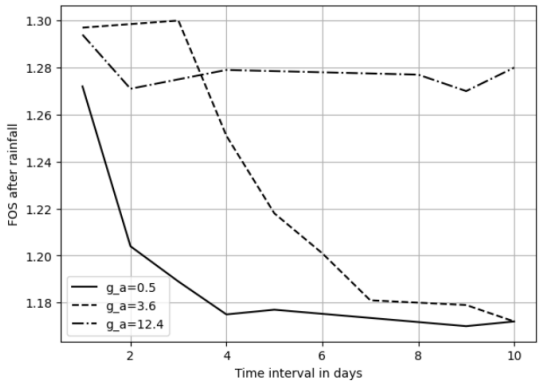

(a) $g_n = 1.09$

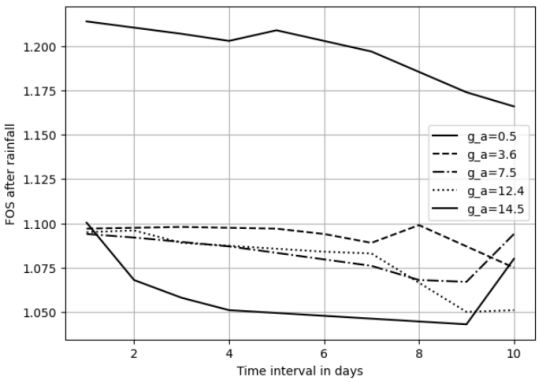

(b) $g_n = 1.48$

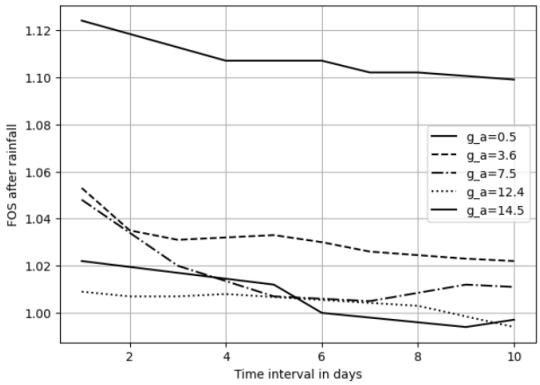

(c) $g_n = 1.89$

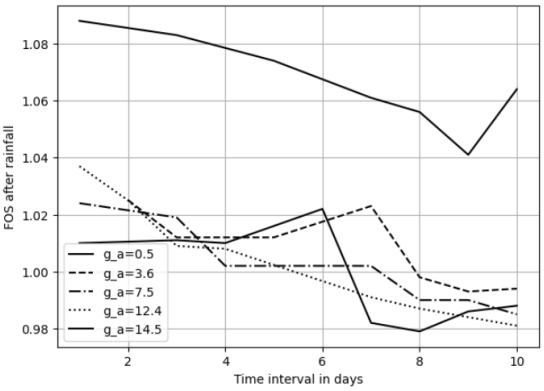

(d) $g_n = 2.28$

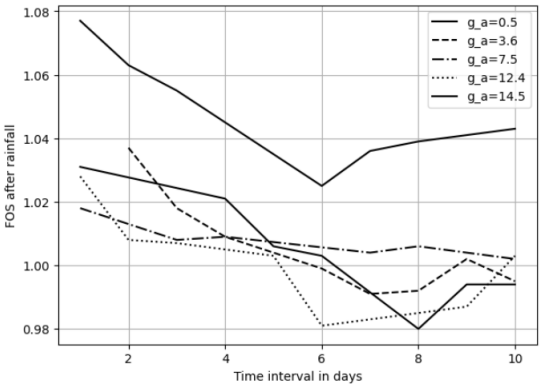

(e) $g_n = 2.68$

Figure 5.9: Effect of g_a values on the FOS of the slope measured for 10 days of time-interval

5.4 Results for Sensitivity Analysis

To investigate the effect of geometry and shear strength parameters on slope stability, the unsaturated slope is analyzed by varying both the slope angle and the friction angle. The impact of geometry is examined by reducing the original slope angle and iterating through three distinct angles: $\theta = 20°$, $25°$ and $30°$. To assess the influence of soil strength parameters on the factor of safety, different friction angles are considered: $\phi = 25°$, $30°$ and $35°$. For each modified slope geometry, achieved by varying the slope angle and height, the slope is analyzed using each selected shear strength parameter. Additionally, the sensitivity of geometry and shear strength parameters is analyzed for the stability of the unsaturated slope across all 25 combinations of VG parameters. This analysis aims to investigate the stability of the unsaturated slope under various VG parameters during a 10-day rainfall period, while also examining the influence of slope geometry and shear strength parameters. The effect of VG parameters: $g_a = 0.5$ and g_n values= 1.09, 1.48, 1.89, 2.28, 2.68 on the FOS of the unsaturated slope for varying slope and friction angles is illustrated in the *figure 5.10*. The graph is created using the Python library matplotlib, showing the relationship between FOS and a 10-day interval of rainfall infiltration. The graph clearly shows that as the slope angle increases, the FOS decreases. Additionally, when the slope angle is held constant, increasing the friction angle results in a increase in the FOS. The maximum factor of safety is recorded for the largest friction angle 35° and the smallest slope angle 20° in all sets of values. Furthermore, it is evident that the FOS gradually decreases with the progression of rainfall infiltration from day 1 to day 10 . Additionally, it is noted that the highest FOS=1.4 of the unsaturated slope after 10 days of infiltration is observed for the lowest VG parameters: $g_a = 0.5$ and g_n=1.09.

The *figure 5.10* (a), (b) demonstrate that for a fixed g_a value of 0.5 and g_n values of 1.09, 1.48 the soil mass collapses entirely when the friction angle ϕ is set to 25° and the slope angle θ is 30°. While in *figure 5.10* (c), (d) and (e) for a fixed g_a value of 0.5 and g_n values of 1.89, 2.28 and 2.68 the soil mass collapses entirely when the friction angle ϕ is set to 25° and the slope angle θ is 25° and 30°. This indicates that with increasing g_n values at the lowest g_a value, increasing slope angles in conjugation with the lowest shear strength parameters result in complete soil mass collapse, highlighting slope instability and the absence of FOS values for these scenarios. This implies that as the slope height increases, it experiences greater gravitational forces, potentially triggering instability due to increased shear stress on the soil. Moreover, in such scenarios, when the slope encounters rainfall, prolonged infiltration results in reducing matrix suction and soil shear strength. Therefore, when the slope heights decrease, soil characteristics with higher shear strength qualities must be developed in order to prevent instability during periods of rainfall.

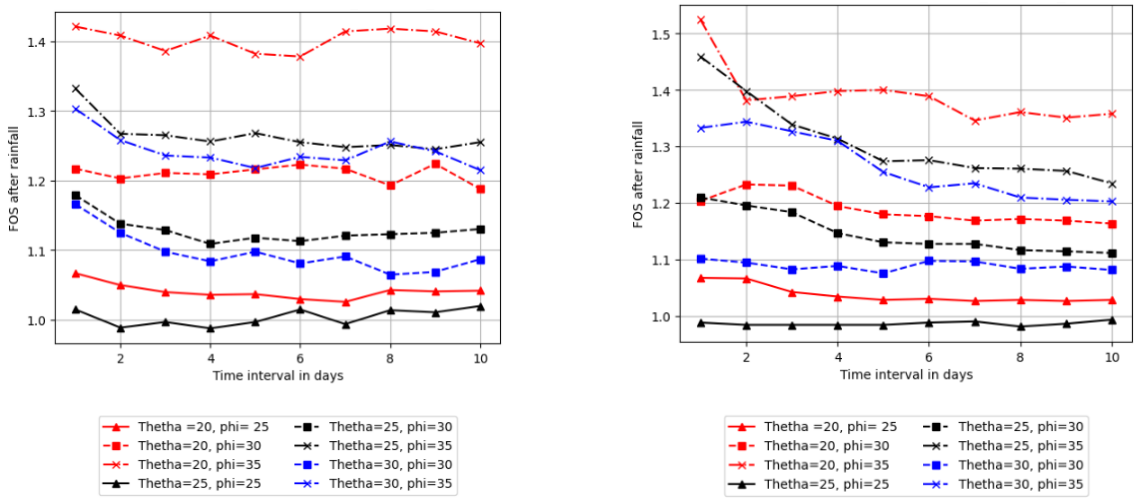

(a) $g_a = 0.5\, g_n = 1.09$

(b) $g_a = 0.5\, g_n = 1.48$

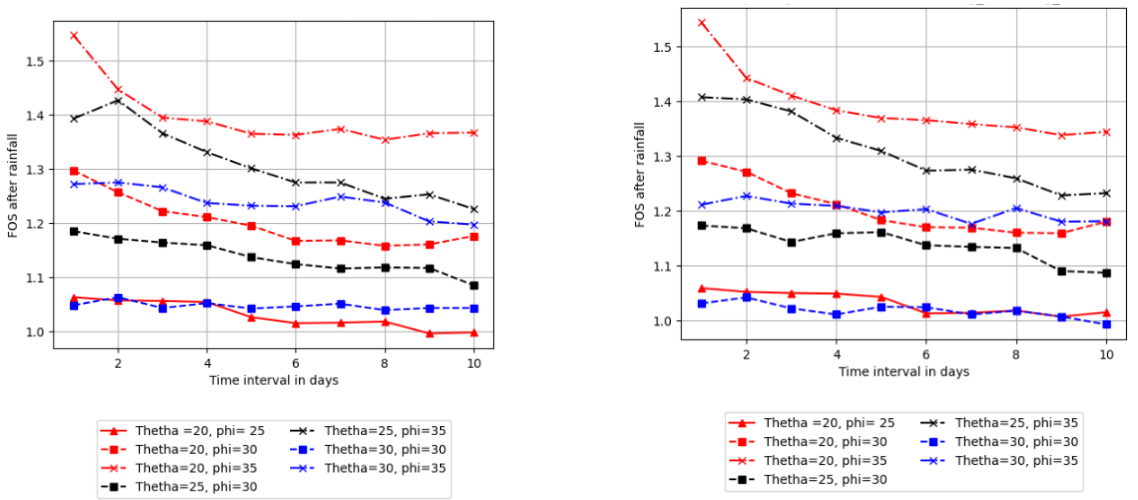

(c) $g_a = 0.5\, g_n = 1.89$

(d) $g_a = 0.5\, g_n = 2.28$

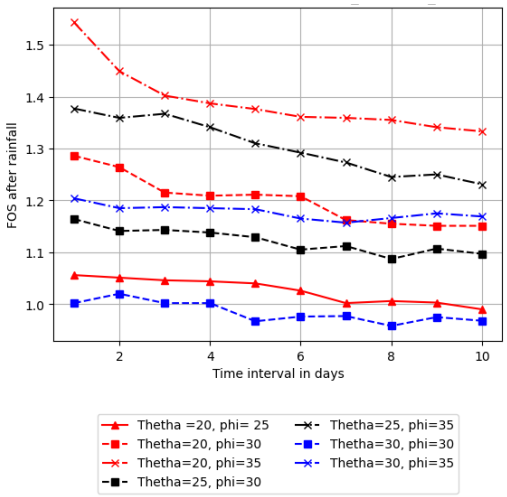

(e) $g_a = 0.5\, g_n = 2.68$

Figure 5.10: Effect of slope geometry and friction angle on slope stability under infiltration

For every distinct slope angle and friction angle, the sensitivity analysis produces 25 graphs when it is analyzed for all 25 combinations of VG parameters. Therefore, for the sake of saving time and optimising the findings, one graph from the remaining four distinct sets of VG parameters is described in the *figure 5.11*. The graphs show the trend of declining FOS as the slope angle rises, with the largest FOS being produced for the highest friction angle when the slope angle is held constant and increased gradually. The *figure 5.10* (b) indicates that the slope fails at slope angle and friction angle: θ= 30°, ϕ = 25° at g_a= 0.5 and g_n = 1.48, whereas the soil body totally collapses at slope angle and friction angle: θ = 25°, ϕ = 25° and θ = 30° , ϕ = 25° in *figure 5.11* (a) with g_a=3.6 and g_n=1.48. The comparison of the findings shows that the slope failure happens significantly earlier than predicted for the lowest friction angle as the g_a values increase gradually for the same g_n value.

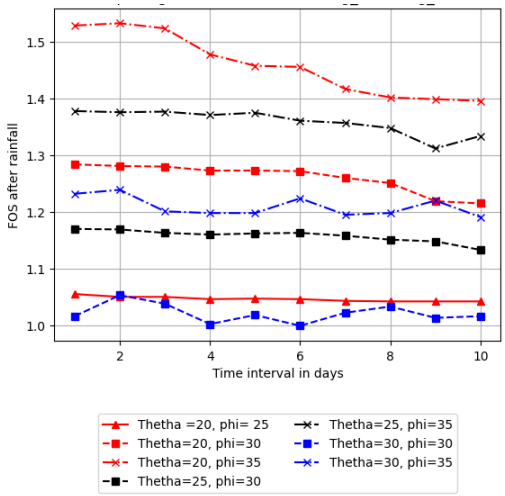

(a) $g_a = 3.6\, g_n = 1.48$

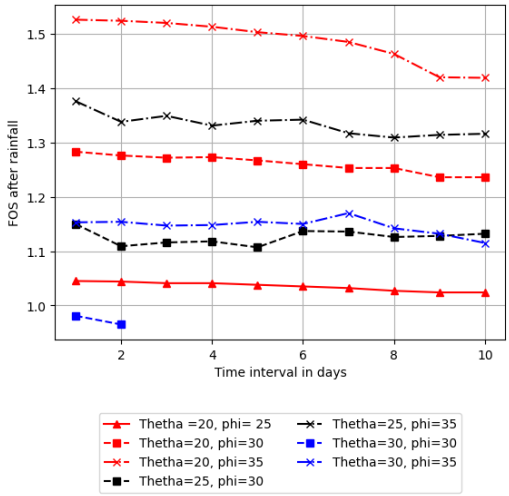

(b) $g_a = 7.5\, g_n = 1.89$

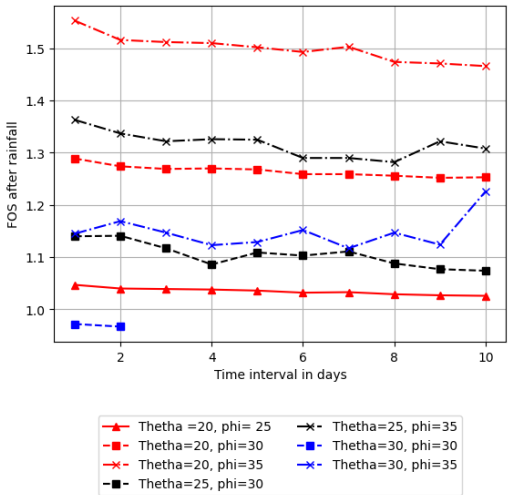

(c) $g_a = 12.4\, g_n = 2.28$

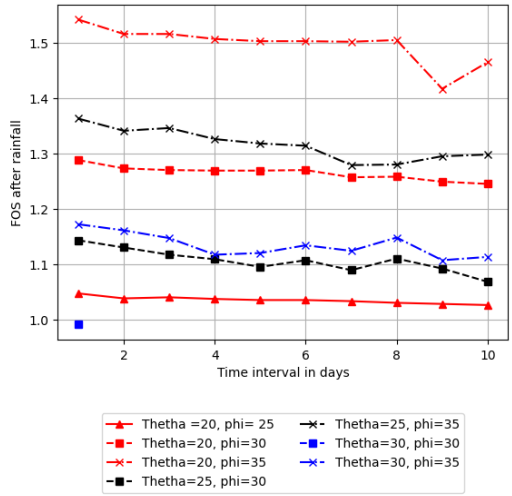

(d) $g_a = 14.5\, g_n = 2.68$

Figure 5.11: Effect of slope geometry and friction angle on FOS under infiltration

Furthermore, the slope offers the best factor safety of all for the largest friction angle and lowest slope angle when it is examined for the highest VG parameters, g_a=14.5 and g_n=2.68 value. This further demonstrates that determining the stability of the unsaturated slope is largely dependent on the VG parameters, slope geometry and shear strength parameters. Therefore, one of these input parameters has to be examined when the slope experiences sudden slope failure from rainfall infiltration while trying to tackle the instability problems by understanding how each parameter is related to the another. Therefore, when subjected to consistent rainfall infiltration, the stability of an unsaturated slope is directly proportional to the VG parameters, shear strength parameters, and inversely related to the slope's geometry.

5.5 Comparison of results

The FOS values evaluated by varying the slope geometry and friction angle under the influence of 10 days of rainfall, are compared with the results of the safety analysis of the slope using the original geometry and shear strength parameters. The FOS values after 10 days of rainfall infiltration for the VG parameters: g_a=0.5 and g_n=1.09 are shown in the table 5.1. Additionally, the table presents the percentage change in the FOS values of the unsaturated slope compared to the FOS value of the original geometry. A negative sign indicates a decrease in FOS value for the corresponding soil properties, while a positive sign indicates an increase. From the table, it is evident that the lowest slope angle for the highest friction angle results in a 19.19% increase in stability under rainfall compared to the original slope geometry and shear strength properties.

Table 5.1: Safety analysis results under infiltration for different scenarios

Parameter	Original slope	Modified slope								
		1	2	3	4	5	6	7	8	9
g_a	0.5	0.5	0.5	0.5	0.5	0.5	0.5	0.5	0.5	0.5
g_n	1.09	1.09	1.09	1.09	1.09	1.09	1.09	1.09	1.09	1.09
θ	32°	20°	20°	20°	25°	25°	25°	30°	30°	30°
ϕ	34°	25°	30°	35°	25°	30°	35°	25°	30°	35°
FOS	1.174	1.042	1.188	1.397	1.02	1.130	1.255		1.087	1.215
Percentage		-11.09%	1.36%	19.19%	-12.96%	-3.54%	7.08%	-	1.08%	1.21%

6
Conclusion

This chapter provides a discussion of the analysis findings and presents a conclusion. Moreover, it includes a comparison of the sensitivity analysis results to identify the key factors that significantly impact the unsaturated slope. Detailed suggestions for future research are also provided, informed by the current investigation data.

6.1 Conclusion

In conclusion, the investigation focused on evaluating the influence of SWCC on the stability of unsaturated slopes under infiltration. The analysis was conducted through complete automation using PLAXIS remote scripting. Every step executed in the software was driven purely by Python code. The assumptions made in determining the VG parameters for iteration and the soil parameters, based on typical range values, did not compromise the accuracy of the results. Moreover, utilizing Python scripts for automated analysis has enhanced the accuracy and dependability of the outcomes. Identifying errors has become seamless due to the automated nature of each step in the process. The primary goal of this study is to automate PLAXIS analysis, allowing for the execution of numerous analyses concurrently. The customized scripts developed are tailored to this particular research and the slope geometry. If these scripts are to be used for varying dimensions or to conduct diverse analyses beyond fully coupled flow deformation and safety assessments in the future, minor adjustments to the code will be necessary, as the scripts are not universally applicable.

The study explores the impact of the SWCC on the stability of an unsaturated slope during infiltration using numerical analysis in PLAXIS 2D, with various Van Genuchten (VG) parameters. The aim is to identify whether g_a or g_n has a greater influence on the FOS under both gravity loading and fully coupled flow-deformation analysis, as well as to evaluate their combined impact on the stability of the slope. The results demonstrate that an increase in g_a and g_n values leads to a decline in FOS, indicating that VG parameters affect slope stability during rainfall events. Additionally, the $g_a$is noted to exhibit higher sensitivity in assessing the stability of the unsaturated slope when compared to $g_n$values. Further, the stability of the slope varies with different VG parameters under initial stress conditions. Nevertheless, changes in groundwater flow parameters can modify the FOS values derived from the numerical analysis. Five distinct sets of VG parameters used in the study were sourced from the PLAXIS manual. The PLAXIS manual presents a series of g_a or

g_n values derived from the USDA approach, serving as the foundation for developing these five unique sets of VG parameters. Consequently, the safety analysis results may fluctuate depending on the varied assumptions made during the VG parameters generation process.

A sensitivity analysis was conducted on the slope geometry, shear strength parameters, and various sets of VG parameters to identify the primary factor influencing slope stability in rainy conditions. The findings reveal that slope angle and height have an inverse relationship with FOS, while the friction angle exhibits a direct correlation with FOS values. The assessment highlights the friction angle as the most critical parameter for assessing the stability of an unsaturated slope. In comparison to the original slope geometry and shear strength parameters, it was determined that, regardless of the VG parameter, combining the lowest slope angle with the highest friction angle notably enhances FOS values during rainfall occurrences compared to the original slope configuration. It's worth mentioning that the original slope angle is 32°, and the sensitivity analysis on slope geometry only considered slope angle values lower than this initial setting. One important limitation of this investigation is that the impact of increasing the slope angle from its original value was not assessed.

6.2 Recommendations

The following recommendations are proposed for the future research investigations:

- The stability of the unsaturated slope in this current study was evaluated under a constant rainfall intensity. To enhance the accuracy of the findings, assessing the slope using time-dependent rainfall data would better simulate real-life conditions.
- The investigation focused solely on evaluating the stability of unsaturated silt slopes. Therefore, additional research can include analyzing unsaturated slopes with different soil types like sand and clay using the same VG parameters established across five unique sets and rainfall data. Furthermore, the FOS values obtained from these investigations can be compiled for comparison to determine how the SWCC impacts various soil types.
- In future studies, the deformation of the slope can be investigated in conjunction with safety analysis by introducing a surcharge load at the top of the slope.
- The current study does not consider the effects of fluctuations in the groundwater table. Hence, a subsequent investigation could explore how varying groundwater table levels during rainfall events affect the stability of the unsaturated slope, thus providing insights into its influence on slope stability.

Bibliography

Abed, A., & Vermeer, P. (2006). Foundation analyses with unsaturated soil model for different suction profiles. *ResearchGate*. https://doi.org/10.1201/9781439833766.ch79

Abramson, L. W., Sharma, S., Lee, T. S., & Boyce, G. M. (2002). *Slope stability and stabilization methods*. John Wiley; Sons,Inc.

Azmi, M., Ramli.M.H, Hezmi.M.A, Yusoff.S.A.N, M., & Alel.M.N.A. (2016). Estimation of soil water characteristic curves (swcc) of mining sand using soil suction modelling. *IOP Conf. Series: Materials Science and Engineering*. https://doi.org/10.1088/1757-899X/527/1/012016

Bentley. (2015). Plaxis 2d-material model manual. *Connect Edition V20.02*.

Bentley. (2020). Plaxis 2d-reference manual. *Connect Edition V20.02*.

Brandell, T., & Sellden, A. (2022). *The effects of severe rainfall on the stability of natural slopes- a numerical analysis of a slope in hjärtum-lilla edet*.

Briaud, J.-L. (2023). *Geotechnical engineering: Unsaturated and saturated soils*. John Wiley Sons, Inc.

Budhu, M. (2010). *Soil mechanics and foundations*. John Wiley; Sons, Inc.

Cai, F., & Ugai, K. (2004). Numerical analysis of rainfall effects on slope stability. *International Journal of Geomechanics*.

Carsel, R. F., & S.Parrish, R. (1988). Developing joint probability distributions of soil water retention characteristics. *Water Resources Research*.

Chin, K. B., Leong, E. C., & Rahardjo, H. (2010). A simplified method to estimate the soil-water characteristic curve. *Canadian Geotechnical Journal*. https://doi.org/10.1139/T10-033

C.W.Fetter. (1988). *Applied hydrogeology*. Merrill PUblishing Company.

Delwyn.G.Fredlund, H.Raharjio, & M.D.Fredlund. (2012). *Unsaturated soil mechanics*. John Wiley Sons, Inc.

Duncan, J. M., Wright, S. G., & Brandon, T. L. (2014). *Soil strength and slope stability*. John Wiley; Sons,Inc.

E.C.Leong, H. R. (1997). Review of soil-water characteristic curve equations. *Journal of Geotechnical and Geoenvironmental engineering*.

Fan, C.-C., & Zeng, R.-Y. (2016). Effect of characteristics of unsatuarted soils on the stability of slopes subject to rainfall. *Japanese Geotechnical Society*.

Gebreyohannes, D., E.Getahun, & Jothimani, M. (2024). Slope stability assessment in the seismically and landslide-prone road segment of gerese to belta, rift valley, ethiopia. *PLOS ONE*. https://doi.org/10.1371/journal.pone.0296807

Girijavallabhan, C. V., & Reese, L. C. (1968). Finite-element method for problems in soil mechanics. *Journal of the Soil Mechanics and Foundations Division*. https://doi.org/10.1061/JSFEAQ.0001107

Gofar, N., & Rahardjo, H. (2016). Saturated and unsaturated stability analysis of slope subjected to rainfall infiltratio. *MATEC Web of Conference, SICEST*. https://doi.org/10.1051/matecconf/201710105004

Gunduz, B. (Lund University). *Analysis of settlements of test embankmenets during 50 years- a comparison between field measurements and numerical analysis*.

Hong, W.-T., Jung, Y.-S., Kang, S., & Lee, J.-S. (2016). Estimation of soil-water characteristic curves in multiple-cycles using membrane and tdr system. *Materials*.

Huvaj, N., Ahmadiadli, M., KartalToker, N., & Kurkcu, M. G. (2012). Comparative study of soil water characteristic curve prediction methods. *3rd International Conference on New Developments in Soil Mechanics and Geotechnical Engineering*.

Janbu, N. (1973). *Slope stability computations*. Technical University of Norway, Institute of Geotechnics; Foundation Engineering.

J.B.Burland, J. (1962). Limitations of the use of effective stresses in partly saturated soils. *Geotechnique*.

Kareem, A., & Fadhil, S. H. (2018). Prediction of soil water characteristic curve using artificial neural network: A new approach. *MATEC web of Conference*. https://doi.org/https://doi.org/10.1051/matecconf/201816201014

Lees, A. (2016). *Geotechnical finite element analysis- a practical guide*. ICE Publishing.

lin Xiong, Y., lin Ye, G., Xie, Y., Ye, B., Zhang, S., & Zhang, F. (2019). A unified constitutive model for unsaturated soil under monotonic and cyclic loading. *Acta Geotechnica*.

Lu, N., & J.Likos, W. (2004). *Unsaturated soil mechanics*. John Wiley Sons, Inc.

N.Radhakrishnan & Lymon.C.Reese. (1970). A review of applications of the finite element method of analysis to problems in soil and rock mechanics. *Elsevier, Soil and Foundations*. https://doi.org/10.3208/sandf1960.10.3_95

Öberg, A. L. (1997). *Matrix suction nin silt and sand slopes* [Doctoral dissertation, Chalmers University of Technology, Department of Geotechnical Engineering].

Pham, H. Q., & G.Fredlund, D. (2003). A practical hysteresis model for the soil-water characteristic curve for soils with negligible volume change. *Geotechnique*.

Rahardjo, H., Kim, Y., & Satyanaga, A. (2019). Role of unsaturated soil mechanics in geotechnical engineering. *International Journal of Geo Engineering*.

R.F.Craig. (1983). *Soil mechanics*. Van Nostrand Reinhold (UK) Co.Ltd.

R.H.McCuen, W.J.Rawls, & D.L.Brakensiek. (1981). Statistical analysis of the brooks -corey and the green-ampt parameters across soil textures. *Water Resources Research*.

Roy, S., & Bhalla, S. K. (2017). Role of geotechnical properties of soil on civilengineering structures. *Resources and Environment*.

S.K.Vanapalli. (2009). Shear strength of unsatuarted soils and its applications in geotechnical engineering practice. *4th Asia Pacific Conference on unsaturated soils, Newcastle, Australia*.

Terzaghi, K. (1942). *Theoretical soil mechanics*. John Wiley Sons, Inc.

Ti, K. S., Huat, B., Noorzaei, J., & Sew, G. S. (2017). A review of basic soil constitutive models for geotechnical application. *EJGE*.

Tremblay, M. (1996). *Modelling of groundwater conditions in silts and fine sands* (tech. rep.). Swedish Geotechnical Institute.

Ullah, S., Khan, M. U., & Rehmana, G. (2020). A brief review of the slope stability analysis methods. *Geological Behaviour*. https://doi.org/10.26480/gbr.02.2020.73.77

USDA. (2016). *Part 652:irrigation national engineering handbook -south california irrigation guide* (tech. rep.). United States Department of Agriculture.

VNS.Murthy. (2003). *Geotechnical engineering- principles and practices of soil mechanics and foundation engineering*. Marcel Dekker Inc.

Yang, H., Rahardjo, H., Leong, E. C., & Fredlund, D. (2004). Factors affecting drying and wetting soil-water characteristic curves of sandy soils. *Canadian Geotechnical Journal*. https://doi.org/10.1139/T04-042

Zhai, Q., Rahardjo, H., Satyanaga, A., & Dai, G. (2019). Estimation of unsaturated shear strength from soil–water characteristic curve. *Acta Geotechnica*. https://doi.org/https://doi.org/10.1007/s11440-019-00785-y(0123456789().,-volV)(0123456789().,-volV)

Z.Zhang, F.Y.Liu, X.G.Zhao, & D.Zhou. (2013). A soil water characteristic curve model considering void ratio variation with stress. *Journal of Hydraulic Engineering*.

A

Appendix 1

A.1 Capillary fringe

Table A.1: Capillary fringe for distinct soil type (Tremblay, 1996)

Type of soil	Height of capillary fringe, m
Silt	1.50-12.0
Clay	> 10.0
Fine sand	0.30 -3.50
Medium Sand	0.12 - 0.50
Coarse Sand	0.03 - 0.15

A.2 Water content

Gravimetric water content is the ratio between mass of water to mass of solid particles and defined as in equation A.1

$$w = \frac{M_w}{M_s} \tag{A.1}$$

Volumetric water content is the ratio between the volume of water to total volume of soil solids and defined as in equation A.2

$$\theta = \frac{V_w}{V_v + V_s} \tag{A.2}$$

Degree of saturation is the ratio between the volume of water to volume of voids in the soil and defined as in equation A.3

$$S = \frac{V_w}{V_v} \tag{A.3}$$

A.3 Empirical Models

The most popular empirical equations that describe the mechanical behaviour of unsaturated soil using SWCC are presented in table A.2 (Delwyn.G.Fredlund et al., 2012).

Table A.2: Empirical equations for SWCC

Researcher	Empirical equation	
Gardner (1958a)	$w(\psi) = \frac{w_s}{1 + a\psi^n}$	(1)
Brooks and Corey (1964)	$\psi = a\left(\frac{w_s}{w}\right)^{\frac{1}{n}}$	(2)
Brutsaert (1967)	$w(\psi) = \frac{1}{1 + \left(\frac{\psi}{a_b}\right)^{n_b}}$	(3)
Van-Genuchten (1980)	$w(\psi) = \frac{w_s}{[1 + (a\psi)^n]^m}$	(4)
Mualem (1976)	$w(\psi) = \frac{w_s}{[1 + (a\psi)^n]^{1-\frac{1}{n}}}$	(5)
Burdine (1953)	$w(\psi) = \frac{w_s}{[1 + (a\psi)^n]^{1-\frac{2}{n}}}$	(6)
McKee and Bumb (1984)	$w(\psi) = exp\left[\frac{a_{m1} - \psi}{n_{m1}}\right]$	(7)
McKee and Bumb (1987)	$w(\psi) = \frac{1}{1 + \exp\left(\frac{\psi - a_{m2}}{n_{m2}}\right)}$	(8)
Fredlund and Xing (1994)	$C(\psi) = \frac{w_s}{\left[\ln\left[e + (\frac{\psi}{a})^n\right]\right]^m}$	(9)

A.4 Effective stress calculation

Table A.3: Effective stress distribution using Terzaghi and Bishop Method

Method	Level	Pore water Pressure u_w	Effective stress $\sigma_{v'}$
Terzaghi	A-A'	-10 kPa	$\sigma_v - u_w$ = 0-(-10) = 10 kPa
	B-B'	0 kPa	$\sigma_v - u_w$ = 18-(0)+ 10 = 28 kPa
	C-C'	10 kPa	$\sigma_v - u_w$ = 20-(10)+ 28 = 38 kPa
Bishop	A-A'	-10 kPa	$\sigma_v - \chi u_w$= 0-0.3(-10)= 3 kPa
	B-B'	0 kPa	$\sigma_v - \chi u_w$= 18-(0)+3= 21 kPa
	C-C'	10 kPa	$\sigma_v - \chi u_w$= 20-1(10)+21= 31 kPa

A.5 Specific gravity values for different soil types

Table A.4: Specific gravity values for different soil types (Roy and Bhalla, 2017)

Type of soil	Specific Gravity, G
Sand	2.65 - 2.67
Silty Sand	2.67 - 2.70
Inorganic Clay	2.70 -2.80
Soil with mica or iron	2.75 - 3.00
Organic Soil	1.00 - 2.60

A.6 Methods to calculate FOS

Limit equilibrium method, forces and moment equilibrium are the three different methods by which the factor of safety of a slope can be evaluated. The methods are represented in *Figure A.1*

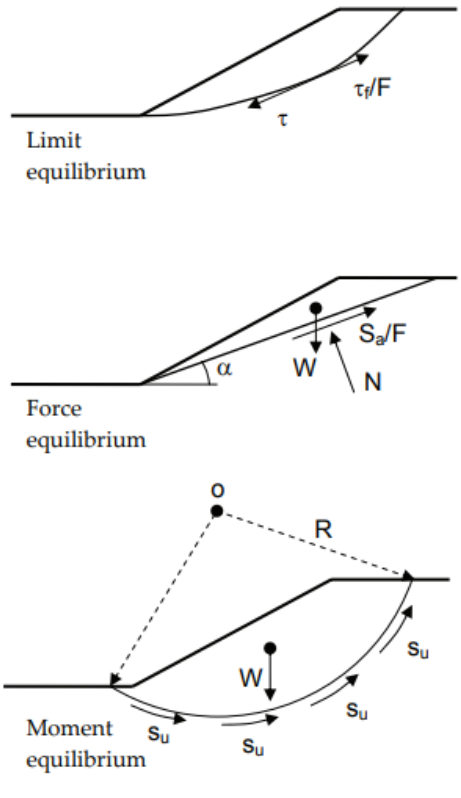

Limit equilibrium:

$$F = \frac{s_u}{\tau} \quad \text{(Total stress)}$$

$$F = \frac{c' + \sigma' \tan \phi'}{\tau} \quad \text{(Effective stress)}$$

Force equilibrium:

$$F = \frac{\text{Sum of resisting forces}}{\text{Sum of driving forces}}$$

$$F = \frac{S_a}{W \sin \alpha} = \frac{\text{cL+Ntan}\phi}{\text{Wsin}\alpha}$$

where,

L = total length of the sliding plane

Moment equilibrium:

$$F = \frac{\text{Sum of resisting moments}}{\text{Sum of driving moments}}$$

$$F = \frac{R \int_0^L s_u dl}{W.x}$$

Figure A.1: Different ways to calculate FOS (Abramson et al., 2002)

A.7 Typical Poisson's ratio for different soil types

Table A.5: Typical Poisson's ratio for different soil types (Budhu, 2010)

Type of soil	Poisson's ratio, μ
Sand	0.15-0.4
Dense	0.2- 0.4
Coarse	0.15
Fine	0.25
Silt	0.3-0.35
Clay	0.1 - 0.5
Saturated	0.4 - 0.5
Unsaturated	0.1 - 0.3
Sandy Clay	0.2 - 0.3

A.8 Young's Modulus values for different types of soil

Table A.6: Young's Modulus values for different types of soil (Budhu, 2010)

Type of soil	Young's Modulus, E_s(N/mm^2)
Sand	
Silty	7-21
Loose	10-24
Dense	48-81
Silt	2-20
Clay	
Very soft	2-15
Soft	5-25
Medium	15-50
Hard	50-100
Sandy	25-250
Glacial till	
Loose	10-153
Dense	144-720
Very Dense	478 -1440

A.9 Water retention curve for silt

The water retention curves obtained in the laboratory is represented by (•), while the matrix suction values measured using piezometers in the laboratory is represented by (∘) and values measured in field are represented by (□).

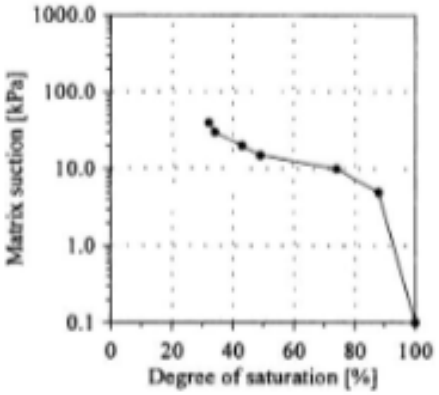

Figure A.2: Water retention curve (Öberg, 1997)

A.10 Annual Precipitation data

Table A.7: Annual Precipitation data used in analysis (Öberg, 1997)

Month	Precipitation (mm/day)	Precipitation (m/day)
January	25	0.0008
February	80	0.0027
March	55	0.0018
April	0	0
May	0	0
June	15	0.0005
July	25	0.0008
August	45	0.0015
September	55	0.0018
October	35	0.0012
November	50	0.0017
December	30	0.0010

B

Appendix 2

B.1 Python Code for PLAXIS 2D-Remote Scripting

```
1
2 Here is the Python code included from an external file:
3 import plxscripting
4 import plxscripting.easy
5
6 from plxscripting.easy import*
7
8 s_i, g_i = new_server('localhost', 10000, password='akshu1234')
9 s_i.new()
10
11 g_i.SoilContour.initializerectangular(0, 0, 125, 65)
12
13 polygon_g = g_i.polygon((0, 0), (0, 54), (24, 54), (88.57, 13.0),
    (125, 13), (125, 0))[0]
14
15 g_i.gotosoil()
16
17 material = g_i.soilmat("Identification", "Siltlayer", "SoilModel",
    "Mohr-Coulomb","Drainagetype","Drained", "gammaUnsat", 16, "
    gammaSat", 19, "eInit", 0.64, "nInit", 0.39,"ERef", 15000, "phi"
    , 34, "nu", .35, "cRef", 3, "GroundwaterClassificationType", "
    User-defined", "SWCCFittingMethod", "Van Genuchten","
    SaturationResidual", 0,"SaturationSaturated", 1,"GenuchtenGn",
    2.06, "GenuchtenGa", .859,"GenuchtenGl", 0, "
    PermHorizontalPrimary", .726624, "PermVertical", .726624)
18
19 g_i.gotostructures()
20 g_i.setmaterial(material)
21
22 GWFlowBaseBC_1= g_i.line((0, 0), (125, 0))[-1]
23 g_i.gwfbc(GWFlowBaseBC_1, "Behaviour", "Closed")
24
25 GWFlowBaseBC_2= g_i.line((0, 0), (0, 54))[-1]
26 g_i.gwfbc(GWFlowBaseBC_2, "Behaviour", "Seepage")
27
28 GWFlowBaseBC_3= g_i.line((125, 0), (125, 13))[-1]
29 g_i.gwfbc(GWFlowBaseBC_3, "Behaviour", "Seepage")
30
31 g_i.gotomesh()
32 print(g_i.mesh(0.03))
33
```

```
g_i.viewmesh()

g_i.gotoflow()
waterlevel_s = g_i.waterlevel((0, 29), (19, 29), (88.57, 13), (125, 13))

g_i.gotostages(True)

phase0_s = g_i.InitialPhase
phase1_s = g_i.phase(phase0_s)
phase2_s= g_i.phase(phase0_s)
phase3_s = g_i.phase(phase2_s)
print(phase1_s, phase2_s, phase3_s)

# To set the loading type for each phase
phase0_s.DeformCalcType = phase0_s.DeformCalcType.gravityloading
phase0_s.Deform.IgnoreSuction = False


phase1_s.DeformCalcType = phase1_s.DeformCalcType.safety
phase1_s.Deform.IgnoreSuction = False

phase2_s.DeformCalcType = phase2_s.DeformCalcType.
   fullycoupledflowdeformation
phase2_s.TimeInterval = 30

phase3_s.DeformCalcType = phase3_s.DeformCalcType.safety
phase3_s.Deform.IgnoreSuction = False

g_i.setcurrentphase(phase0_s)
g_i.Polygons[0].activate(phase0_s)

precipitation = g_i.precipitation
g_i.precipitation.Discharge.set(phase2_s, 0.0027)
g_i.precipitation.HeadMinimum.set(phase2_s, -30)
phase2_s.Deform.UseDefaultIterationParams = False
phase2_s.Deform.MaxSteps = 10000
phase2_s.Deform.DesiredMinIterations = 15
phase2_s.Deform.DesiredMaxIterations = 30

g_i.precipitation.activate(phase2_s)

print(g_i.calculate(phase0_s, phase1_s,phase2_s, phase3_s))


values = [phase1_s.echo(), phase3_s.echo()]
names = ["phase1", "phase3"]
for values, name in zip(values, names):
    print("*", name, "*")
    for v in values.split("  "):
        if v.startswith("SumMsf"):
            print("\t" + v.rstrip("\r\n"))
    print("#" * 40)
print('/' * 40)
```